

Scalar advection schemes for ocean modelling on unstructured triangular grids

William Paul Budgell · Anabela Oliveira · Morten D. Skogen

Received: 1 December 2006 / Accepted: 30 May 2007 / Published online: 25 July 2007
© Springer-Verlag 2007

Abstract Several schemes for scalar advection on unstructured triangular grids are assessed for possible use in ocean modelling applications. Finite element, finite volume and finite volume–element approaches are evaluated. A series of tests, including a numerical order of convergence analysis, idealized rotating cone and cylinder experiments, and transport of a tracer through the Stommel Gyre representation of ocean basin-scale circulation, are carried out. Volume element Eulerian–Lagrangian and third-order Runge–Kutta discontinuous Galerkin schemes are recommended for use in tracer studies. Taylor–Galerkin and second-order Runge–Kutta discontinuous Galerkin are found to be robust and accurate second-order schemes. When positivity is required, a fluctuation redistribution scheme was found to be an easily implemented, accurate, and computationally efficient approach.

Keywords Advection algorithms · Unstructured grid · Finite elements · Ocean modeling

Responsible editor: Phil Dyke

W. P. Budgell (✉) · M. D. Skogen
Institute of Marine Research, P.O. Box 1870, Nordnes,
5817 Bergen, Norway
e-mail: paul.budgell@imr.no

W. P. Budgell · M. D. Skogen
Bjerknes Centre for Climate Research, Bergen, Norway

A. Oliveira
Núcleo de Estuários e Zonas Costeiras,
Departamento de Hidráulica e Ambiente,
Laboratório Nacional de Engenharia Civil,
Av. do Brasil, 101, 1700-066 Lisboa, Portugal

1 Introduction

Increasing interest in ocean modeling with unstructured grids has developed over the past few years. Unstructured finite element (Greenberg et al. 1998; Le Provost et al. 1994; Le Roux and Staniforth 2000; Lynch and Werner 1987, 1991), finite volume (Chen and Beardsley 2002; Oksuzoglu and Hees 1998), and spectral element (Curchitser et al. 2001; Iskandarani et al. 1995; Levin et al. 2000) approaches are now employed in a variety of ocean modelling applications. One of these models, denoted Quoddy (Lynch and Werner 1991), has proven highly successful on wind- and tidally dominated coastal and continental shelf problems (Hannah et al. 2001; Lynch and Hannah 2001; Lynch et al. 1996). However, when we began to address tracer transport problems using Quoddy, limitations associated with the treatment of advection in the model became evident. Excessive diffusion was required to suppress under- and overshooting due to dispersive ripples in the presence of sharp concentration gradients. In an attempt to address these shortcomings, we have conducted a review of advection schemes suitable for use on unstructured triangular grids.

Several excellent texts have appeared over the past 10 years or so on the subject of numerical treatment of advection and hyperbolic problems. Among these, Hirsch (1990), LeVeque (1992), and Toro (1999), while addressing finite difference approaches, provide valuable background on the issues involved with numerical treatment of advection problems. Finlayson (1992) and Morton (1996) include excellent overviews of finite element approaches using unstructured triangular grids. Godlewski and Raviart (1996), Kröner (1997), and

LeVeque (2002) provide comprehensive descriptions of finite volume methods, including those suitable for use on triangular unstructured grids. Vreugdenhil and Koren (1993) is an extensive comparison of a wide variety of schemes for advection–diffusion problems, including finite element and finite volume approaches. These texts provided an excellent background for the literature review and examination of specific algorithms. This review includes analyses of recent monotonic finite volume, discontinuous Galerkin and Eulerian–Lagrangian schemes not covered by the listed texts.

Recently, Hanert et al. (2004) analyzed continuous, non-conforming, and discontinuous finite element and finite volume approaches to ocean scalar advection. They included analyses of dispersion and mass conservation characteristics that complement the analyses in this study. This study includes a broader range of advection schemes currently in use in engineering fields, particularly monotonic and Eulerian–Lagrangian schemes.

The paper is organized as follows. In Section 2, the schemes examined in the study are described. Section 3 contains a description of the test cases and the results of the tests. Relative computational performance of the schemes is discussed in Section 4. The paper

concludes in Section 5 with a summary of results and conclusions.

2 Advection schemes

From the vast literature relevant to the study of scalar advection on unstructured triangular grids, we have selected a number of representative schemes that are of interest to the ocean modeling community. Pure advection of a passive scalar is addressed in this study, expressed as the two-dimensional advection equation:

$$\frac{\partial c}{\partial t} + u \cdot \nabla c = 0 \quad (1)$$

with Dirichlet boundary conditions on the inflow part (Γ_1) of the boundary (Γ)

$$c(x, t) = c_b(x, t), \quad x \in \Gamma_1$$

where c is concentration, u is the advecting velocity, t is time, and c_b is the specified boundary forcing. It should be noted that in this study, the flow will be assumed to be incompressible. Thus, in the scalar situation, the advection and conservation forms of Eq. 1 are equivalent because the velocity field is nondivergent.

Table 1 Abbreviations, descriptions, and key references for advection schemes examined

Abbreviation	Description	References
GFEM	'classic' Galerkin finite element method	Morton (1996)
NQ-RK2	nodal quadrature finite element with second-order Runge-Kutta	Morton (1996)
NQ-EF	nodal quadrature finite element with Euler forward	Morton (1996)
SUPG	streamline upwind Petrov–Galerkin	Brooks and Hughes (1982)
SUPG–Tri	modified streamline upwind Petrov–Galerkin	Mizukami (1985)
SUPG–MH	modified streamline upwind Petrov–Galerkin	Mizukami and Hughes (1985)
TG	Taylor–Galerkin	Donéa (1984)
PSI	positive streamwise invariant cell vertex finite volume	Deconinck et al. (1994)
FE-FCT	finite element flux-corrected transport	Löhner et al. (1987)
Lax–Wendroff	Lax–Wendroff cell vertex finite volume	Deconinck et al. (1994)
Fluct. Redis.	fluctuation redistribution cell vertex finite volume	Hubbard and Roe (2000)
VELA	control-volume finite element Eulerian–Lagrangian	Oliveira (1997)
VELA–FCT	VELA with flux-corrected transport	Oliveira and Fortunato (2002)
VELA–N–LF	VELA with non-linear filter	Oliveira and Fortunato (2002)
MLG	maximum limited gradient cell-centered finite volume	Batten et al. (1996)
MUST	monotonic upwind scheme for triangles cell-centered finite volume	Tamamidis (1995)
RKDG2	second-order Runge–Kutta discontinuous Galerkin without limiter	Cockburn and Shu (1998)
RKDG2–minmod	RKDG2 with minmod limiter	Cockburn and Shu (1998)
RKDG2–TVBM	RKDG2 with total variance bounded in the means limiter	Cockburn and Shu (1998)
RKDG3	third-order Runge–Kutta discontinuous Galerkin without limiter	Cockburn and Shu (1998)
RKDG3–minmod	RKDG3 with minmod limiter	Cockburn and Shu (1998)
RKDG3–TVBM	RKDG3 with total variance bounded in the means limiter	Cockburn and Shu (1998)
MPDATA2	MPDATA finite difference, two iterations, non-oscillatory	Smolarkiewicz and Margolin (1998)
MPDATA3	MPDATA with three iterative passes, non-oscillatory	Smolarkiewicz and Margolin (1998)

The schemes applied in this study to solve Eq. 1, together with their abbreviations and key references, are summarized in Table 1. The schemes are briefly described in 1. Further details on the various schemes can be obtained from Budgell and Skogen (2000) and the original references.

We have broadly categorized the advection algorithms and listed the algorithms in each category as follows:

- *Galerkin finite element*: GFEM, NQ-RK2, NQ-EF, TG
- *Stabilized Galerkin methods*: SUPG, SUPG–Tri, SUPG–MH
- *Fluctuation distribution*: PSI, Lax-Wendroff, Fluc. Redis.
- *Flux-corrected transport*: FE-FCT
- *Cell-centered finite volume*: MLG, MUST
- *Discontinuous Galerkin*: RKDG2, RKDK2-minmod, RKDG2-TVBM, RKDG3, RKDK3-minmod, RKDG3-TVBM,
- *Eulerian–Lagrangian methods*: VELA, VELA–FCT, VELA–NLF

The final scheme applied in this study is not a triangular unstructured-grid advection scheme at all—it is a structured-grid, finite-difference scheme applied to regular, square-grid cells. The finite difference scheme is included to provide a basis of comparison for finite difference ocean modelers unfamiliar with unstructured grid techniques. Multidimensional positive definite advection transport algorithm (MPDATA) is commonly used in general ocean circulation models (Bleck et al. 1992; Higdon 2002). Hecht et al. (1995, 2000) and Hasumi (1999) found MPDATA to be among the best of the schemes they tested in their comparison studies.

It should be noted that several of the schemes, such as the finite volume, discontinuous Galerkin and VELA methods, have been designed with flux conservation in mind. The benefits of employing such conservation measures will not be evident in this study, as we only consider scalar advection in nondivergent flow fields.

3 Comparison of advection schemes

The performance of the schemes described in the previous section is examined in a series of test problems. The first of the problems is a numerical order of convergence analysis that tests the rate at which the various advection schemes approach an exact, smooth solution with successive mesh refinement. The reduction in the order of accuracy produced by slope and flux limiters can be determined, as can the sensitivity to grid orien-

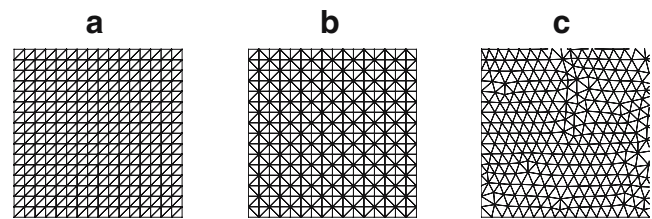


Fig. 1 Grid types

tation and connectivity. The second test is a rotating cone problem. This problem tests peak and shape preservation. Positivity, monotonicity, and the ability to preserve sharp gradients is tested by the rotating cylinder problem. The final problem is the advection of a Gaussian hill within an analytic basin-scale ocean circulation, the Stommel gyre. This case tests the ability of the schemes to properly represent tracer advection in a strongly deformed flow field typical of ocean circulation. By conducting the Stommel gyre tracer experiment on both a homogeneous-resolution grid and on a locally refined grid, it is also possible to determine which of the advection schemes benefit most from local mesh refinement.

Some of the schemes can exhibit a sensitivity to grid orientation and connectivity. To test sensitivity to mesh characteristics, tests were run on the three different types of grid (Fig. 1).

Grid A is a right-triangle mesh with a constant orientation of the diagonal at 45° from the lower left to the upper right. It is a regular grid in that each interior node is always attached to six elements. Grid B is a “Union Jack” grid, in which nodes alternate between being connected to four and eight triangular elements. Some schemes display degraded accuracy on this type of variable connectivity. Grid C is an unstructured grid produced by a mesh generator. The mesh is isotropic in that there is no preferred mesh orientation. Interior nodes are generally attached to six triangular elements, but some are connected to as few as four and others to as many as eight triangles. Grid C is typical of meshes generated for realistic applications.

3.1 Order of convergence

The various schemes are tested for the rate at which they converge to the exact solution. While the meshes used to test convergence are regular, the analysis will provide an indication of which schemes are likely to benefit most from local grid refinement in a general unstructured mesh. A scheme with a very poor convergence rate will derive relatively little benefit from local refinement, for example, and thus, may not be a very competitive candidate for use in a general

unstructured mesh. Furthermore, whereas the schemes can often approach or achieve nominal orders of accuracy in the absence of limiting operations, convergence rates can drop markedly if slope or flux limiters are applied to maintain monotonicity. An order of convergence analysis can show which of the monotonic, or nearly monotonic, schemes can maintain high accuracy as indicated by the convergence rate.

The test problem is that described by Hubbard (1999) and Hubbard and Roe (2000). The initial concentration field is a double sine wave:

$$c = \sin(2\pi x)\sin(2\pi y) \quad (2)$$

with a velocity $u = (1, 2)^T$ on a doubly periodic domain $[0, 1] \times [0, 1]$. At $t = 1.0$, the concentration field should have returned to its initial value. Changes in the L_1 norms as the meshes are refined from 17×17 through 129×129 grid nodes are recorded as numerical order of convergence (NOC) estimates in Table 2 for grid A.

The VELA schemes were not included in this test because space- and time-varying boundary conditions were not implemented in the model. Instead, grid refinement experiments were conducted on the rotating

cone problem, and the results will be discussed in the next section.

The time steps used were selected to satisfy the Courant stability criterion with a time step of approximately 0.8 of the maximum permitted by linear stability analysis for the explicit schemes and a Courant number of approximately 0.8 for the implicit schemes. For GFEM, SUPG, SUPG–Tri, SUPG–MH, PSI, Lax–Wendroff, Fluct. Redist., and MPDATA, a time step of $\Delta t = 0.32\Delta x_{\min}$ was used, where Δx_{\min} is the minimum element side length. For NQ-RK2, TG, FE-FCT, MLG, and MUST, $\Delta t = 0.16\Delta x_{\min}$ was used; for RKDG2, $\Delta t = 0.08\Delta x_{\min}$; for RKDG3, $\Delta t = 0.04\Delta x_{\min}$; and for NQ-EF, $\Delta t = 0.02\Delta x_{\min}$.

The tables show that the GFEM, NQ-RK2, SUPG, TG, FE-FCT, Lax–Wendroff, Fluct. Redis., and RKDG2 are all second-order schemes and that RKDG3 is a third-order scheme. As expected, the PSI scheme is first order. The SUPG–Tri, SUPG–MH, MLG, MUST, MPDATA2, and MPDATA3 schemes are no better than first order, sacrificing second-order accuracy for improved monotonicity. NQ-EF does not achieve second order accuracy because of its first-order time discretization. It is noteworthy that, whereas, as shown in the next section, the FE-FCT and Fluct. Redis. schemes are monotonic, these schemes retain second-order rates of convergence on smooth problems. Applying the minmod limiter to RKDG2 does not degrade the convergence rate appreciably; the convergence rate remains nearly second order. However, when the minmod limiter is applied to RKDG3, the convergence rate becomes second order, as well. Thus, if it is necessary to apply the minmod limiter to ensure monotonicity, there is no advantage in using the higher order RKDG3 over the RKDG2 scheme.

Most of the schemes are insensitive to the grid orientation and connectivity. The exceptions are MLG (as noted by Hubbard 1999) and MUST. These schemes degrade in performance on grid B relative to grid A, with NOC values on grid B of 0.82 and 0.42, respectively, for 65×65 to 129×129 nodes.

Nearly all the schemes exhibit consistent behavior as resolution is increased from 17×17 through 33×33 , 65×65 to 129×129 nodes. The exceptions are the RKDG–TVBM schemes. The TVBM limiter is designed to provide a combination of the unlimited and minmod properties. Figure 2 shows how this affects the convergence rates. At coarse spatial resolutions (17×17 and 33×33), the RKDG2–TVBM results follow those of the unlimited RKDG2, whereas at higher resolutions (65×65 and 129×129), the RKDG2–TVBM results follow those of RKDG2–minmod. The

Table 2 Numerical order of convergence (NOC) of the schemes on the right-triangle (A) grids based on L_1 scores in refining from 17×17 to 33×33 , 33×33 to 65×65 and 65×65 to 129×129 grid nodes

Advection scheme	NOC		
	17–33	33–65	65–129
GFEM	2.07	2.01	2.00
NQ-RK2	1.89	1.99	2.00
NQ-EF	1.88	1.86	1.59
SUPG	1.98	1.99	2.00
SUPG–Tri	0.50	0.71	0.84
SUPG–MH	0.95	0.95	0.97
Taylor–Galerkin	1.97	1.99	2.00
PSI	0.54	0.65	0.79
FE-FCT	2.44	2.34	2.02
Lax–Wendroff	1.86	2.01	2.02
Fluctuation redistribution	1.83	1.99	2.01
MLG	1.00	1.24	1.49
MUST	0.44	0.77	0.69
RKDG2 no limiter	2.46	2.28	2.14
RKDG2 minmod	1.89	2.00	1.93
RKDG2 TVBM	2.08	–	1.60
RKDG3 no limiter	3.23	3.07	3.03
RKDG3 minmod	1.94	1.98	1.89
RKDG3 TVBM	–	–	1.77
MPDATA2 non-oscillatory	0.90	1.10	1.20
MPDATA3 non-oscillatory	1.09	1.19	1.29

MPDATA2 and MPDATA3 are on square finite difference grids.

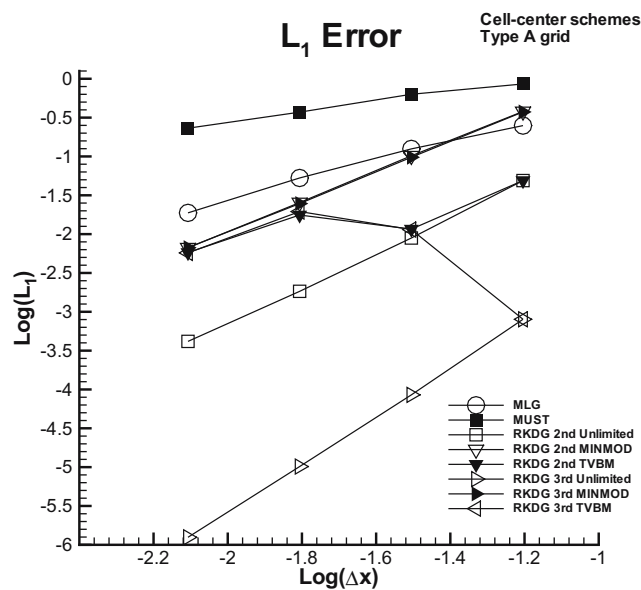


Fig. 2 L_1 norms for the cell-centered schemes on grid A meshes

RKDG3–TVBM results, on the other hand, are the same as RKDG3 unlimited at 17×17 , the same as RKDG2 unlimited at 32×32 and follow RKDG3–minmod and RKDG2–minmod for 65×65 to 129×129 resolution. Where the TVBM results leave, the unlimited curve and switch to the minmod curve is largely determined by the parameter M in (3.7) in Cockburn and Shu (1998). Unless stated otherwise, their value of $M = 50$ is also used in this study.

Whereas the NOC estimates for most of the schemes appear to have converged by 129×129 nodes, some of the schemes, notably RKDG2/3 TVBM, NQ-EF,

SUPG–Tri, PSI, MLG, and MPDATA2/3, may need further mesh refinement to provide stable estimates.

3.2 Rotating cone

All the schemes were applied to the rotating cone problem described by Hubbard (1999) and Hubbard and Roe (2000). The initial condition is a cone defined by:

$$c = \begin{cases} \cos^2(2\pi r) & \text{for } r \leq 0.25 \\ 0 & \text{otherwise,} \end{cases} \quad (3)$$

where $r^2 = (x + 0.5)^2 + y^2$ and the velocity $\mathbf{u} = (-2\pi y, 2\pi x)^T$ is applied to the domain $[-1, 1] \times [-1, 1]$, with zero concentration specified on the inflow boundary conditions. At $t = 1.0$, the cone should have returned to its initial position without change of shape after one revolution. The schemes were applied to grids A, B, and C.

The spatial discretization is 65×65 nodes, for a minimum grid size of 0.03125. The time step for GFEM, SUPG, SUPG–Tri, SUPG–MH, PSI, Lax–Wendroff, Fluct. Redis., and MPDATA was $\Delta t = 0.08\Delta x_{\min}$. For NQ-RK2, TG, FE-FCT, MLG, and MUST, $\Delta t = 0.04\Delta x_{\min}$ was used; for RKDG2, $\Delta t = 0.03\Delta x_{\min}$, for RKDG3, $\Delta t = 0.02\Delta x_{\min}$ and for NQ-EF $\Delta t = 0.01\Delta x_{\min}$. The VELA schemes were integrated using 5- and 50-time steps per simulation (NT = 5 and 50, where NT is the number of time steps in the integration), so that the corresponding time steps are 0.2 and 0.02, respectively.

The results are summarized in Table 3 and the results for grid C are shown in Figs. 3, 4, and 5.

Table 3 Rotating cone test case results at $t = 1.0$ on grid C. MPDATA2 and MPDATA3 are on a square finite difference grid

Advection scheme	Min	Max	L_1	Advection scheme	Min	Max	L_1
GFEM	-0.032	0.995	0.222	MLG	0.000	0.854	0.124
NQ-RK2	-0.237	0.855	1.384	MUST	0.000	0.977	0.388
NQ-EF	-0.281	0.896	1.548	RKDG2	-0.011	0.977	0.049
SUPG	-0.012	0.931	0.146	RKDG2-minmod	0.000	0.747	0.176
SUPG–Tri	-0.003	0.493	0.762	RKDG2-TVBM	-0.011	0.977	0.049
SUPG–MH	-0.003	0.759	0.339	RKDG3	-0.002	0.997	0.003
TG	-0.019	0.989	0.049	RKDG3-minmod	0.000	0.749	0.168
PSI	0.000	0.321	1.386	RKDG3-TVBM	-0.002	0.997	0.004
FE-FCT	0.000	0.711	0.297	MPDATA2	0.000	0.591	0.604
Lax-Wendroff	-0.208	0.836	1.122	MPDATA3	0.000	0.805	0.347
Fluct. Redis.	0.000	0.849	0.551				
VELA (NT = 50)	-0.008	0.985	0.025				
VELA (NT = 5)	-0.006	0.994	0.007				
VELA–FCT (NT = 50)	0.000	0.985	0.014				
VELA–FCT (NT = 5)	0.000	0.994	0.005				
VELA–NLF (NT = 50)	0.000	0.984	0.024				
VELA–NLF (NT = 5)	0.000	0.994	0.024				

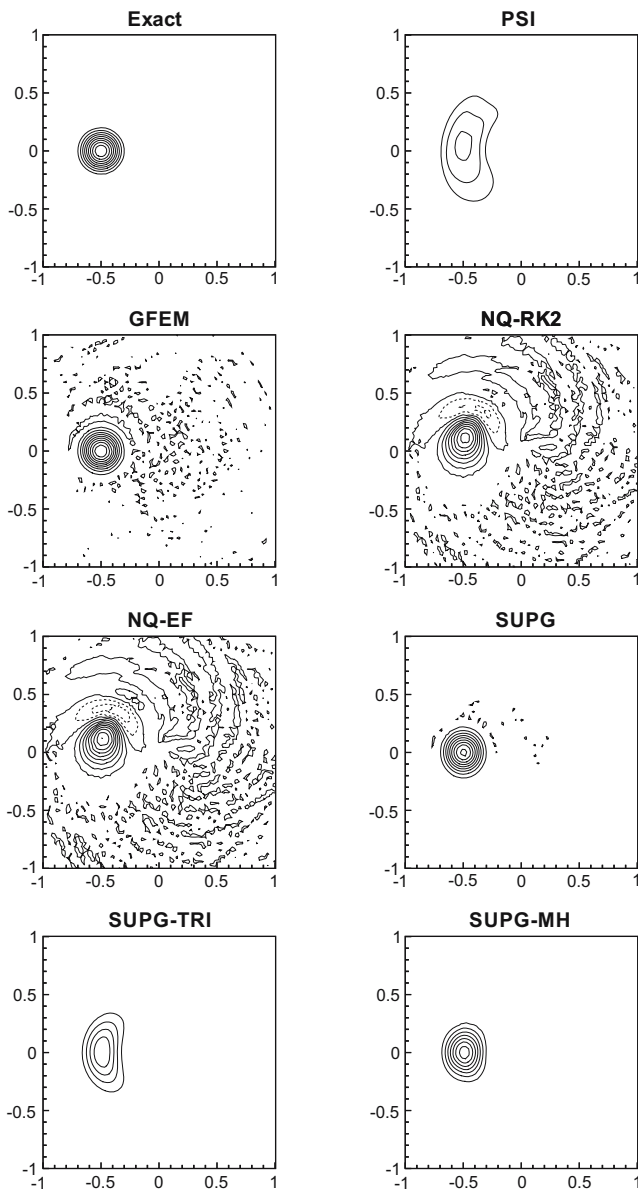


Fig. 3 Concentrations at $t = 1.0$ for the schemes in the rotating cone test case on grid C

From Table 3, it can be seen that the RKDG3, RKDG3-TVBM, VELA, VELA-FCT, and VELA-NLF provide the best overall agreement with the exact solution in terms of minimum L_1 values and matching the minimum and maximum. Of the monotonic schemes, the VELA-FCT and VELA-NLF are clearly superior, providing the same level of accuracy as the original VELA. Of the second-order schemes, the TG, RKDG2, RKDG2-TVBM, GFEM, and SUPG provide the lowest L_1 scores while capturing the peak values with slight undershoot. The MUST scheme is monotonic and captures the peak amplitude but at the price of a higher L_1 score. On reasonably well-structured grids, such as grid C, the MLG scheme

provides a good balance of monotonicity, peak capturing, and minimal error. The FE-FCT and Fluct. Redis. schemes are both essentially flux-corrected transport algorithms and exhibit similar behavior. Whereas both are monotonic, the Fluct. Redis. scheme demonstrates less attenuation of the peak amplitude but produces an L_1 score that is nearly double that of FE-FCT. This is due to shape and phase errors in the Fluct. Redis. results (Fig. 4). The results for all the schemes are nearly the same for grids A and C, but the results for MLG, RKDG2–minmod and RKDG3–minmod deteriorate appreciably on grid B, with L_1 values of 0.444, 0.563, and 0.561, respectively.

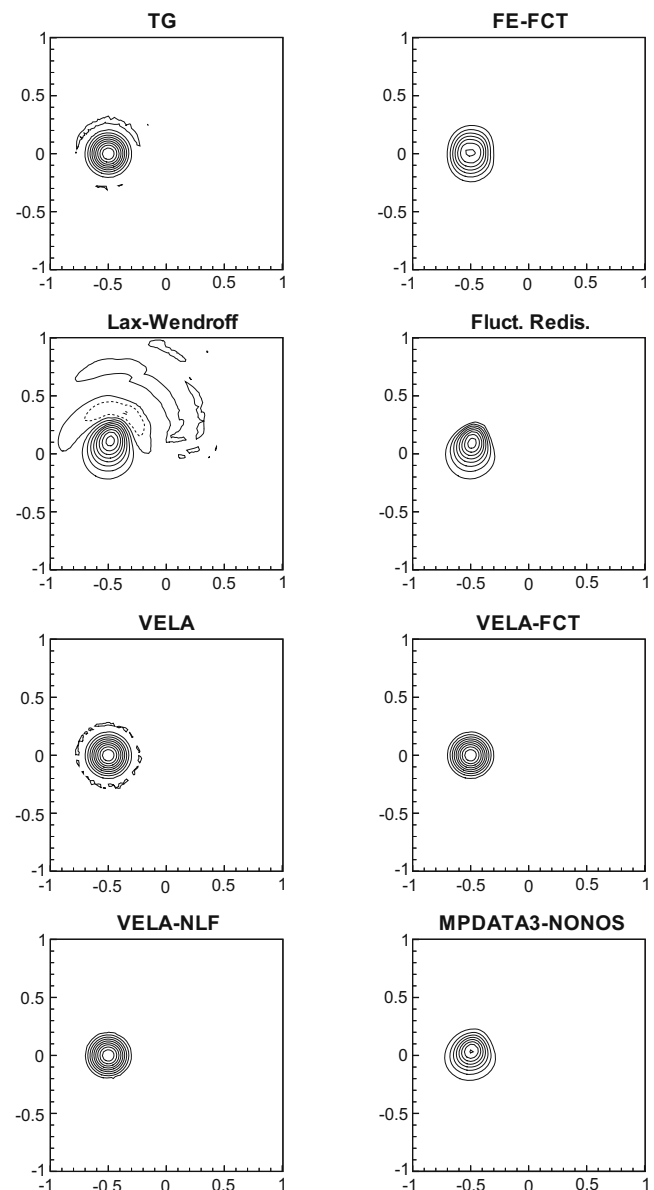


Fig. 4 Concentrations at $t = 1.0$ for the schemes in the rotating cone test case on grid C. The VELA schemes shown have $NT = 5$. MPDATA3 is on a square finite difference grid

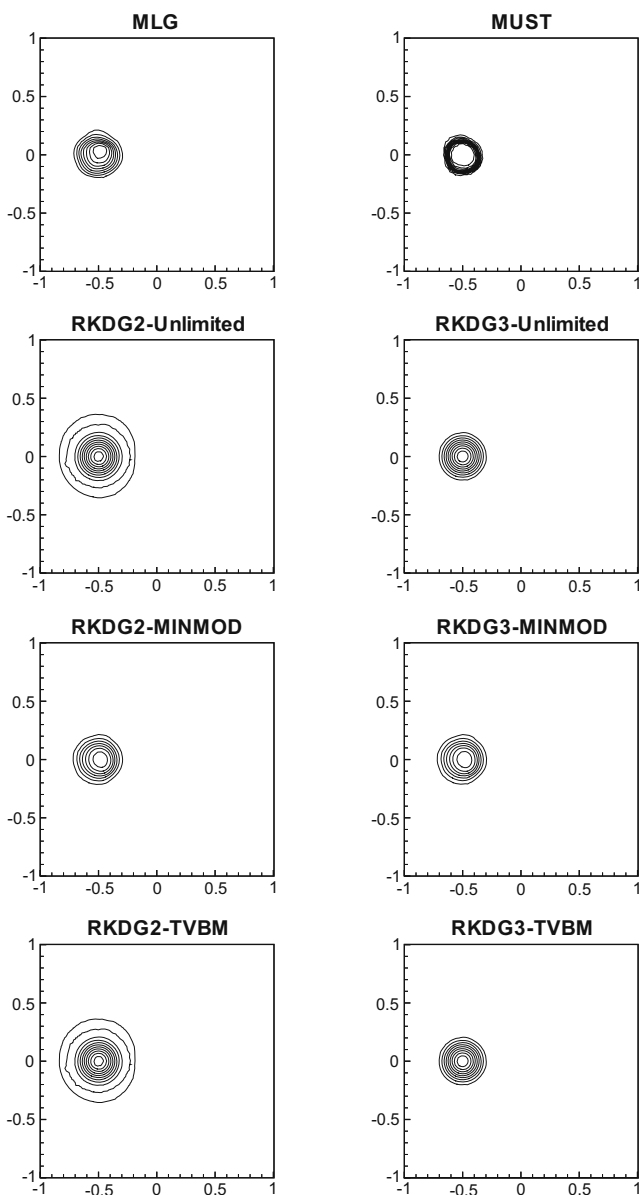


Fig. 5 Concentrations at $t = 1.0$ for the schemes in the rotating cone test case on grid C

As shown in Figs. 3, 4, and 5, RKDG3, RKDG3-TVBM, VELA-FCT, and VELA-NLF are close to the exact solution. The elevated L_1 values exhibited by MUST and Fluct. Redis. would appear to be attributable to the distortion of the cone shape and to phase errors. MUST effectively transforms the cone to a cylinder, whereas Fluct. Redis. retains the distortion evident in the Lax-Wendroff solution. The high L_1 values of NQ-RK2, NQ-EF, and Lax-Wendroff are due to the negative undershoots and dispersive ripples evident in the figures. Attenuation of the cone amplitude causes high L_1 values for the PSI and SUPG-Tri results.

The MPDATA2 non-oscillatory finite difference scheme produces excessive dissipation, but the

Table 4 Numerical order of convergence in the cone test case on the right-triangle (A) grids

Advection scheme	L_1
VELA (NT = 50)	2.89
VELA (NT = 5)	2.30
VELA-FCT (NT = 50)	2.52
VELA-FCT (NT = 5)	2.09
VELA-NLF (NT = 50)	2.94
VELA-NLF (NT = 5)	3.02
TG	2.35
FE-FCT	2.20

MPDATA3 non-oscillatory scheme produces results that are slightly better than Fluct. Redis. and FE-FCT.

The convergence properties of VELA schemes in refining from 65×65 to 129×129 nodes on the rotating cone problem for grid A is shown in Table 4.

Results from the TG and FE-FCT schemes are included to provide a basis for comparison. From the L_1 values, the convergence rates of the VELA-NLF and VELA (NT = 50) schemes are approximately third order, the remainder are roughly second-order.

3.3 Rotating cylinder

To test the monotonicity and robustness of the schemes, they were each applied to the rotating cylinder problem described by Hubbard (1999). The initial condition is a cylinder defined by:

$$c = \begin{cases} 1 & \text{for } r \leq 0.25 \\ 0 & \text{otherwise,} \end{cases} \quad (4)$$

where $r^2 = (x + 0.5)^2 + y^2$ and the velocity $\mathbf{u} = (-2\pi y, 2\pi x)^T$ is applied to the domain $[-1, 1] \times [-1, 1]$, with zero concentration specified on the inflow boundary conditions. At $t = 1.0$, the cylinder should have returned to its initial position without change of shape after one revolution. The grid size and time steps used in this case are the same as described for the rotating cone test.

The results are summarized in Table 5.

From the L_1 , the most accurate schemes are the VELA-FCT with NT = 5, VELA with NT = 5, MUST, and RKDG3. VELA-FCT and MUST are also monotonic. As in the rotating cone case, results on grids A and C are similar, performance degrades appreciably on grid B for MLG, RKDG2-minmod, and RKDG3-minmod, with L_1 values of 0.511, 0.595, and 0.592, and peak values reduced to 0.981, 0.924, and 0.924, respectively. It should be noted, however, that the MLG is the second most accurate second-order scheme

Table 5 Rotating cylinder test case results at $t = 1.0$ on grid C. MPDATA2 and MPDATA3 are on a square finite difference grid

Advection scheme	Min	Max	L_1	Advection scheme	Min	Max	L_1
GFEM	-0.326	1.298	0.905	MLG	0.000	1.000	0.250
NQ-RK2	-0.504	1.547	1.569	MUST	0.000	1.000	0.142
NQ-EF	-0.628	1.739	1.937	RKDG2	-0.057	1.082	0.242
SUPG	-0.165	1.133	0.359	RKDG2-minmod	0.000	0.999	0.313
SUPG-Tri	-0.040	0.835	0.712	RKDG2-TVBM	-0.042	1.059	0.259
SUPG-MH	-0.036	1.001	0.393	RKDG3	-0.101	1.113	0.130
TG	-0.183	1.192	0.330	RKDG3-minmod	0.000	0.999	0.302
PSI	0.000	0.601	1.223	RKDG3-TVBM	-0.012	1.013	0.194
FE-FCT	0.000	1.000	0.444	MPDATA2	0.000	1.000	0.630
Lax-Wendroff	-0.373	1.411	1.021	MPDATA3	0.000	1.000	0.464
Fluct. Redis.	0.000	1.000	0.515				
VELA(NT = 50)	-0.079	1.096	0.203				
VELA (NT = 5)	-0.145	1.143	0.116				
VELA-FCT (NT = 50)	0.000	1.000	0.180				
VELA-FCT (NT = 5)	0.000	1.000	0.104				
VELA-NLF (NT = 50)	0.000	1.000	0.236				
VELA-NLF (NT = 5)	0.000	1.000	0.206				

(after MUST) on grids A and C and is still competitive with all of the monotonic second-order schemes, except MUST, on grid B. GFEM, NQ-RK2, NQ-EF, and Lax-Wendroff produce excessive levels of oscillation. In addition, the Lax-Wendroff and the Fluct. Redis. lead to severe deformation of the cylinder shape. The accuracy of MPDATA3 is comparable to that of FE-FCT, but the accuracy of MPDATA2 is somewhat lower than that of FE-FCT and Fluct. Redis. The accuracy of the TG is also corrupted by significant oscillations. The PSI and the SUPG-Tri results display appreciable errors in the peak amplitude due to excessive numerical diffusion.

3.4 Stommel Gyre

To test the schemes' behavior under conditions typical of basin-scale ocean circulation, the analytical solution for the Stommel gyre (Stommel 1948) was used to advect a Gaussian hill tracer distribution, as described by Hecht et al. (1995, 2000). From Hecht et al. (2000), the stream function representing the circulation pattern of the Stommel Gyre can be expressed as:

$$\Psi = \frac{1}{\rho} \gamma \left(\frac{b}{\pi}\right)^2 \sin\left(\frac{\pi y}{b}\right) (pe^{Ax} + qe^{Bx} - 1), \quad (5)$$

where x and y are distances from the western and southern boundaries, respectively, b is the meridional

dimension of the basin and ρ is the density of the fluid. The parameter γ is defined as

$$\gamma = \frac{F\pi}{rb}, \quad (6)$$

and

$$A = -\alpha/2 + (\alpha^2/4 + (\pi/b)^2)^{1/2}, \quad (7)$$

$$B = -\alpha/2 - (\alpha^2/4 + (\pi/b)^2)^{1/2}, \quad (8)$$

$$p = (1 - e^{B\lambda}) / (e^{A\lambda} - e^{B\lambda}), \quad (9)$$

$$q = 1 - p, \quad (10)$$

$$\alpha = \frac{1}{r} \frac{\partial f}{\partial y}. \quad (11)$$

The zonal width of the basin is $\lambda = 10^4$ km, the depth is $D = 200$ m, the wind stress amplitude $F = 0.1 \text{ N m}^{-2}$, the friction coefficient is $r = 10^{-6} \text{ s}^{-1}$, and the Coriolis parameter is specified as $f = y \times 10^{-11} \text{ m}^{-1} \text{ s}^{-1}$. The meridional dimension of the gyre is $b = 6.3 \times 10^3$ km.

The velocity is obtained from the volume stream function as

$$u = D^{-1} \frac{\partial \Psi}{\partial y}, \quad (12)$$

$$v = -D^{-1} \frac{\partial \Psi}{\partial x}. \quad (13)$$

The initial tracer concentration distribution is Gaussian, with an amplitude of 1, width of $800/\sqrt{2}$ km, and is centered at $(\lambda/3, b/3)$ over a background concentration of 1. The stream function pattern and

initial tracer distribution are shown in Fig. 6. The integration was conducted for a period of 1.5×10^8 s (~ 5 years). The reference solution was obtained through a back-trajectory calculation with a fifth- and sixth-order Runge–Kutta integration using Eqs. 12 and 13.

The problem was solved on two different meshes. The first mesh, shown in Fig. 7, is an unstructured grid with a mean element side length of 108.6 km and consists of 6,588 nodes and 12,724 elements. The MPDATA schemes were applied using a square grid with a grid size of 100 km. For most of the schemes, a time step of 2×10^4 s was used. The exceptions were NQ-EF, RKDG2, and RKDG3 with time steps of 1×10^3 , 1×10^4 and 5×10^3 s, respectively, and the VELA schemes that were run with time steps of 5×10^6 (NT = 30) and 3.75×10^7 s (NT = 4).

The results are summarized in Table 6 and shown in Figs. 8, 9, and 10.

The parameters of Table 6 are those of Hecht et al. (1995) and are used in this study to permit comparison with those results. The parameters include MIN, MAX, l_2 , V and TV , where

$$\text{MIN} = \min\{c\} - \min\{c_R\}, \tag{14}$$

$$\text{MAX} = \max\{c\} - \max\{c_R\}, \tag{15}$$

$$l_2 = \frac{\overline{\{c - c_R\}^2}}{\overline{\{c_R\}^2}}^{\frac{1}{2}}, \tag{16}$$

$$V = \frac{\overline{\{c - \bar{c}\}^2}}{\overline{\{c_R - \bar{c}_R\}^2}} - 1, \text{ and} \tag{17}$$

$$TV = \frac{\overline{\left\{ \left| \frac{\partial c}{\partial x} \right| + \left| \frac{\partial c}{\partial y} \right| \right\}}}{\overline{\left\{ \left| \frac{\partial c_R}{\partial x} \right| + \left| \frac{\partial c_R}{\partial y} \right| \right\}}} - 1, \tag{18}$$

where c is the concentration in the models and c_R is the reference concentration.

With a perfect match to the reference solution, these error diagnostics would have a value of zero. Negative

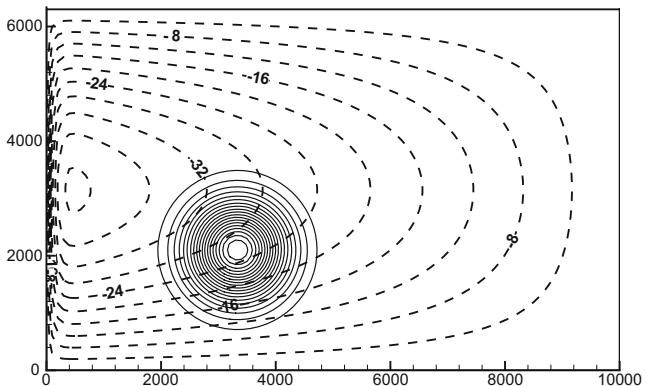


Fig. 6 Streamfunction and initial tracer distribution for the Stommel Gyre case. Streamfunction is in units of $10^6 \text{m}^3 \text{s}^{-1}$. Contour interval of the tracer concentration is 0.05

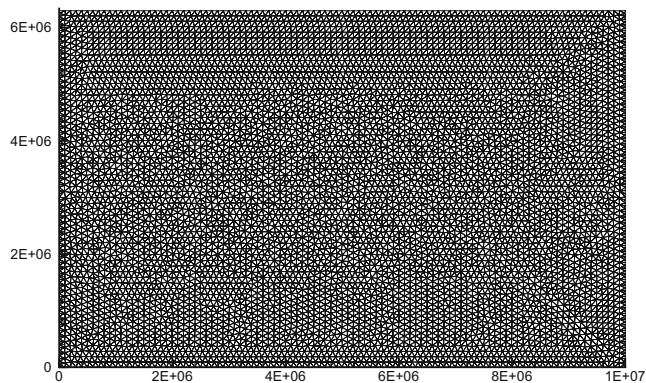


Fig. 7 Unstructured triangular grid used in the Stommel Gyre case

values of MIN indicate undershoot, negative values of MAX indicate attenuation of the peak, and positive values of MAX indicate overshoot. l_2 is indicative of goodness of fit in an L_2 sense, V measures the variance or ‘energy’ of the numerical solution compared to that of the reference solution, and TV is a measure of the magnitude of gradients and small-scale variability in the numerical relative to the reference solution.

Advecting tracer through the strongly deformed velocity field in the western boundary current proves to be a challenging test case. It was not possible to obtain a numerically stable solution with the NQ-EF scheme and, as shown in Fig. 8, NQ-RK2 is extremely noisy, as well. The TG and Lax–Wendroff schemes (Fig. 9) and GFEM (not shown) exhibited considerable small-scale noise in the western boundary region. The noisiness is reflected in large TV values. Only the VELA schemes and RKDG3 closely resemble the reference solution. The VELA (NT=4) schemes (Fig. 9) display the peculiar artifact that a ‘ghost’ strip replicating the leading edge of the tracer field appears across the middle of the tracer distribution. These patterns are due to the large velocities in the western boundary that separate parts of the diffused plume and transport them ahead of the main plume. The VELA schemes with NT=30 produce some low-amplitude small-scale rippling in the concentration contours.

Of the monotonic schemes, VELA–FCT (NT=4) and VELA–NL (NT=4) are clearly superior, as shown by the summary statistics of Table 6. Based on the l_2 scores, the rest of the monotonic schemes in decreasing order of performance are VELA–FCT (NT=30), VELA–NLF (NT=30), MPDATA3, MPDATA2, Fluct. Redis., FE-FCT, PSI, MUST, RKDG3–minmod, RKDG2–minmod, and MLG. The MPDATA schemes are superior to all the monotonic schemes except for VELA–FCT and VELA–NLF. It is interesting to note that, although RKDG3 is one of the best overall

Table 6 Stommel gyre test case results. MPDATA2 and MPDATA3 are on a square grid cell finite difference grid

Advection scheme	MIN	MAX	l_2	V	TV
GFEM	-6.032	0.021	1.117	0.722	18.312
NQ-RK2	-5.416	4.919	3.803	14.703	41.572
NQ-EF	-	-	-	-	-
SUPG	-0.107	-0.711	0.652	-0.712	-0.353
SUPG-Tri	-0.688	-0.411	0.618	-0.349	0.203
SUPG-MH	-0.657	-0.494	0.584	-0.359	0.231
TG	-0.660	-0.386	0.591	-0.266	3.025
PSI	0.000	-0.752	0.729	-0.745	-0.398
FE-FCT	0.000	-0.564	0.666	-0.374	0.076
Lax-Wendroff	-0.367	-0.340	0.582	-0.223	2.152
Fluct. Redis.	0.000	-0.593	0.614	-0.569	-0.089
VELA $NT = 30$	-0.070	-0.238	0.309	-0.231	0.370
VELA $NT = 4$	-0.057	0.003	0.128	-0.019	0.332
VELA-FCT $NT = 30$	0.000	-0.261	0.316	-0.274	0.194
VELA-FCT $NT = 4$	0.000	0.001	0.124	-0.023	0.271
VELA-NLF $NT = 30$	0.000	-0.407	0.422	-0.443	0.201
VELA-NLF $NT = 4$	0.000	-0.016	0.154	-0.042	0.347
MLG	0.000	-0.704	0.754	-0.667	-0.197
MUST	0.000	-0.640	0.735	-0.569	-0.096
RKDG2	-0.139	-0.276	0.355	-0.218	0.086
RKDG2-minmod	0.000	-0.709	0.751	-0.671	-0.223
RKDG2-TVBM	-0.015	-0.667	0.734	-0.649	-0.168
RKDG3	-0.112	-0.132	0.186	-0.115	0.063
RKDG3-minmod	0.000	-0.700	0.749	-0.668	-0.220
RKDG3-TVBM	-0.007	-0.611	0.700	-0.627	-0.135
MPDATA2	0.000	-0.539	0.579	-0.593	-0.091
MPDATA3	0.000	-0.507	0.551	-0.562	-0.053

schemes, by imposing monotonicity through the TVD minmod limiter, the peak concentration amplitude is attenuated to the point that the scheme is nearly the worst. The performance of MLG is surprisingly poor, given that the Stommel mesh is isotropic, and MLG performed well on the cone case on a similar mesh (grid C). The distortions in the concentration field produced by MUST in the cone case are present in this test, as well. MUST successfully maintains strong gradients (and, thus, the relatively small TV value), but at a price of flattening the peak. The PSI and the SUPG schemes are, again, very diffusive.

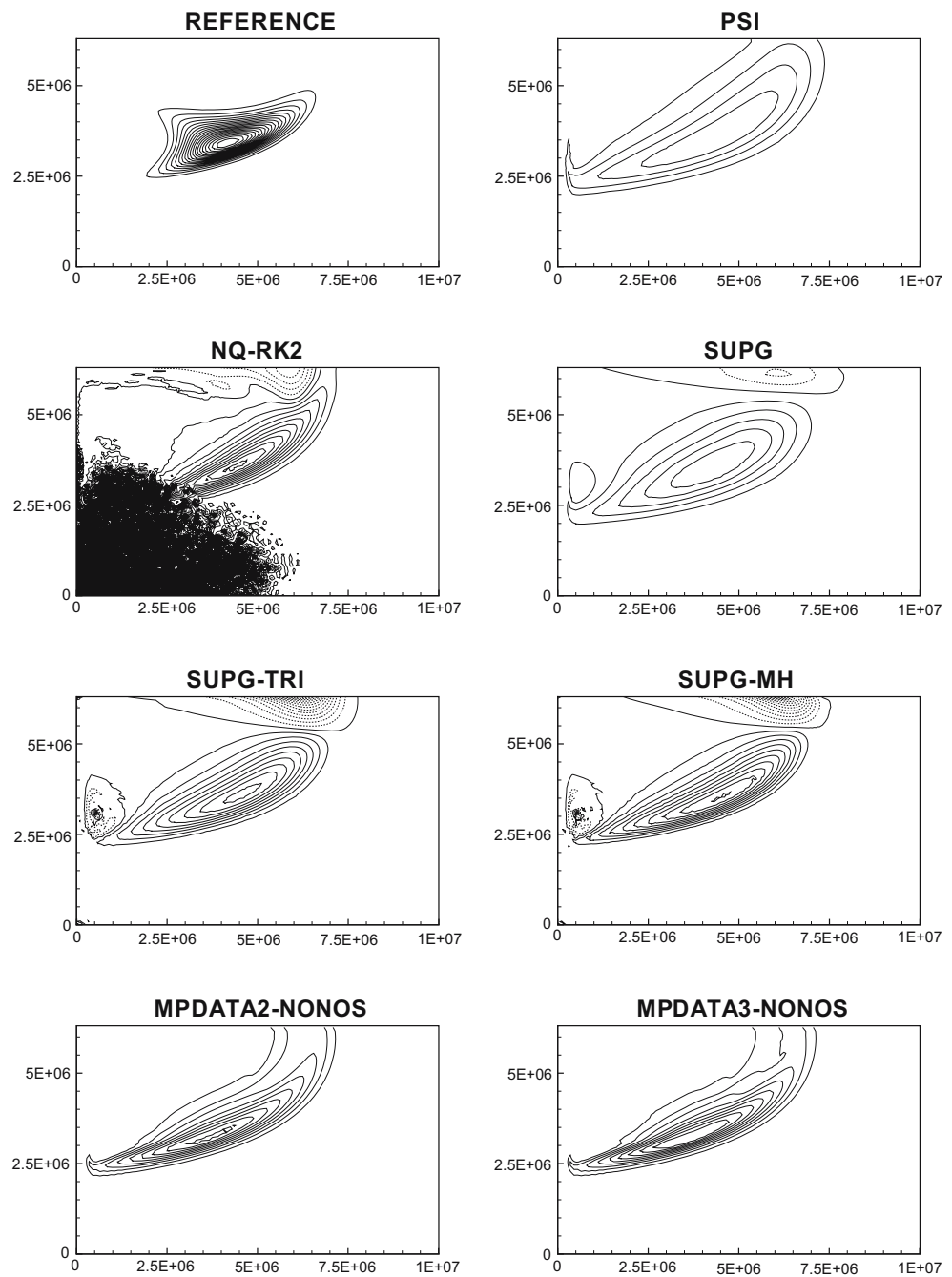
To examine the performance of the various schemes when the mesh is refined to resolve the velocity structure, the stretched mesh shown in Fig. 11 is employed. The grid is stretched such that the element side lengths are inversely proportional to the magnitude of the velocity. The minimum nodal separation on an element is 7.4 km, the maximum is 219 km, and the mean is 74.2 km. The mesh contains 12,524 nodes and 24,062 elements. The time step used with each of the schemes in the stretched mesh case is 0.1 of the value used in the non-stretched case described above.

The results are shown in Table 7 and Figs. 12, 13, and 14. Not surprisingly, the higher-order schemes

converge more rapidly to the reference solution as the grid is refined. The VELA schemes (Fig. 14) and RKDG3 unlimited (Fig. 13) are virtually indistinguishable from the reference solution. The improvement in l_2 values from the uniform mesh to the stretched mesh is most dramatic for these schemes, varying from a ratio of 6.7 for VELA-NLF ($NT=4$) to 19.8 for VELA-FCT ($NT=30$). The ratio of the average grid sizes between the two meshes is 1.46. If a third-order scheme, such as RKDG3, were not producing enhanced accuracy from the local grid refinement, but only from the average grid size reduction, then we would expect a ratio of 3.11. Because the RKDG3 ratio is 10.3, the scheme clearly benefits from local grid refinement. The expected ratio based on average grid size for second-order schemes is 2.13. The TG, Lax-Wendroff, and RKDG2 have ratios of 5.6, 3.9, and 2.7, respectively, displaying good convergence properties.

The performance of SUPG on the stretched grid is disappointing. Its l_2 ratio is only 1.4, which is first-order, at best. This result differs dramatically from that of the numerical order of convergence analysis, in which SUPG achieved second-order rates of convergence. Conversely, the SUPG-Tri and SUPG-MH schemes obtain l_2 ratios of 3.4 and 3.7, respectively, and are

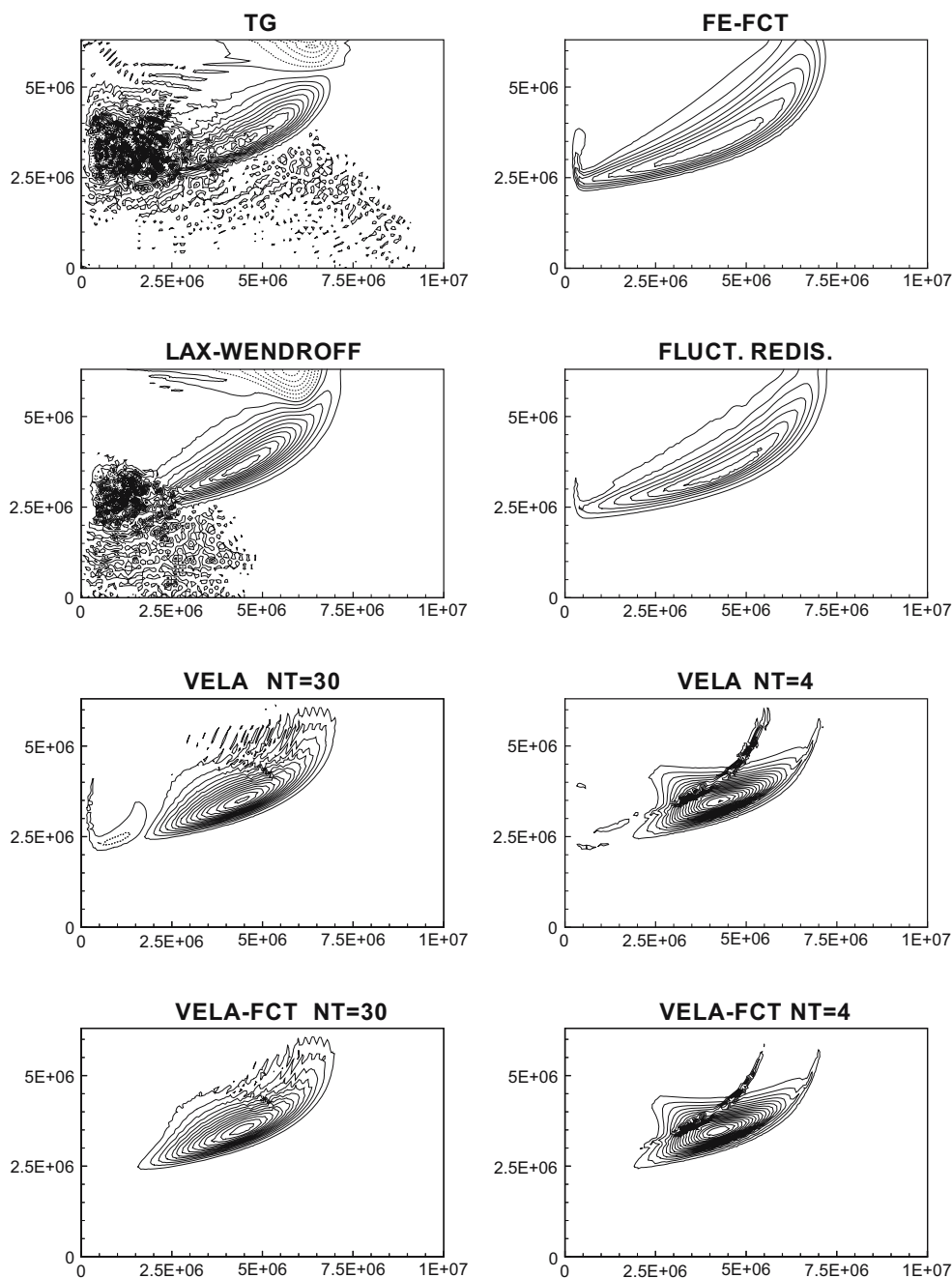
Fig. 8 Concentrations at $t = 1.5 \times 10^8$ s for the reference solution and advection schemes in the Stommel gyre test case. MPDATA2 and MPDATA3 are on a square grid cell finite difference grid



competitive with the formally second-order schemes on the stretched grid. SUPG–Tri, SUPG–MH, and RKDG2 are not monotonic, but their negative undershoot is less than half such second-order schemes as TG and Lax–Wendroff. These two SUPG schemes could be useful candidates for applications that can tolerate a slight negative undershoot. It was not possible to obtain stable numerical solutions for GFEM, NQ-RK2, and NQ-EF, so these schemes were not included in the stretched-grid test case.

Of the monotonic schemes, VELA–FCT and VELA–NLF are clearly superior. The Fluct. Redis. scheme has the next best l_2 score and now displays significantly better accuracy than FE-FCT. This is reflected in the l_2 convergence rates, with a value of 2.1 for Fluct. Redis. and 1.8 for FE-FCT. The rest of the monotonic schemes possess l_2 values between 0.43 to 0.45, except MLG which is much worse with a value of 0.575 and PSI with 0.630, as a result of the high numerical damping. MUST has a l_2 ratio of 1.7,

Fig. 9 Concentrations at $t = 1.5 \times 10^8$ s for advection schemes in the Stommel gyre test case



and the MAX value of -0.014 is much improved over the uniform mesh value of -0.640, indicating excellent reproduction of the peak value. However, MUST still seriously distorts the concentration pattern, as shown in Fig. 13.

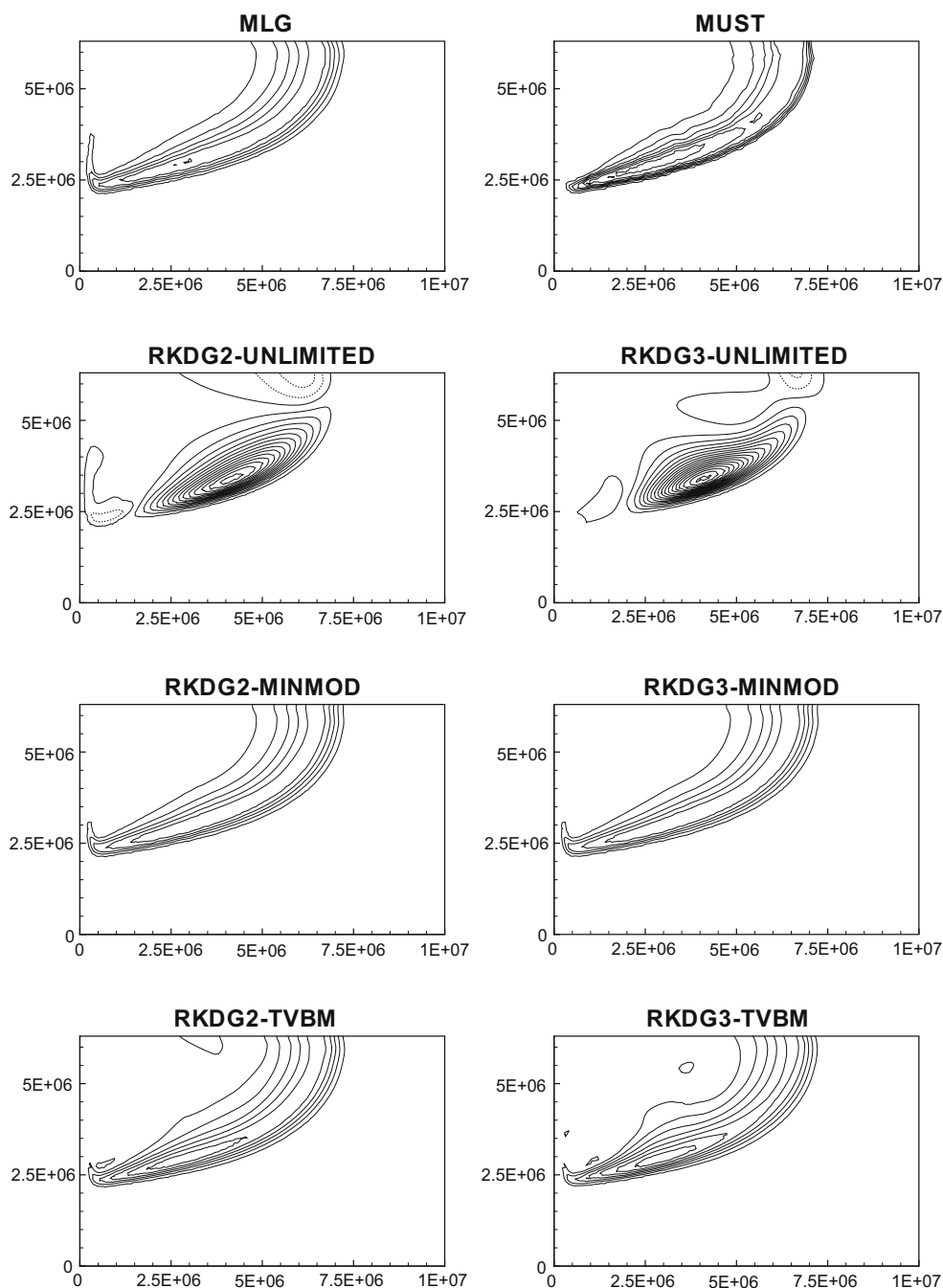
4 CPU time requirements

To obtain a rough indication of relative computing time requirements of the various advection schemes, the 65×65 rotating cone on grid A was run as a

benchmark. The time steps are the same as used before in the 65×65 rotating cone test case. The ratios between the time steps of the various schemes was found to hold for further grid refinement, such as to 129×129 nodes, for example.

Times relative to that of the PSI scheme are listed in Table 8. It should be noted that no attempt was made to optimize the performance of the schemes. The RKDG3 schemes, for example, would benefit from performing a 6×6 matrix reduction in-line as an algebraic expression instead of using calls to external matrix routines. The relative times listed in Table 8 are only intended as

Fig. 10 Concentrations at $t = 1.5 \times 10^8$ s for advection schemes in the Stommel gyre test case



a very approximate guide to the computational requirements of the various methods.

MPDATA2 and Lax-Wendroff are considerably faster than any of the other schemes. Of the monotonic unstructured grid schemes, Fluct. Redis. is the fastest, followed closely by VELA-FCT and VELA-NLT, both with $NT = 5$.

The relatively high computational efficiency achieved by the VELA schemes is accomplished through the large time steps possible due to the absence

of Courant stability restrictions. The CPU times of VELA are dependent on the accuracy required for the tracking, through a closing error, and of the accuracy of the evaluation of the integrals at the feet of the characteristic lines. The values of the closing errors and the number of subdivision triangles used in this study are typical of estuarine applications. Because the velocities of the tests were time-independent, the CPU times for the tracking are very small. We expect that for tests with space- and time-dependent velocities, the

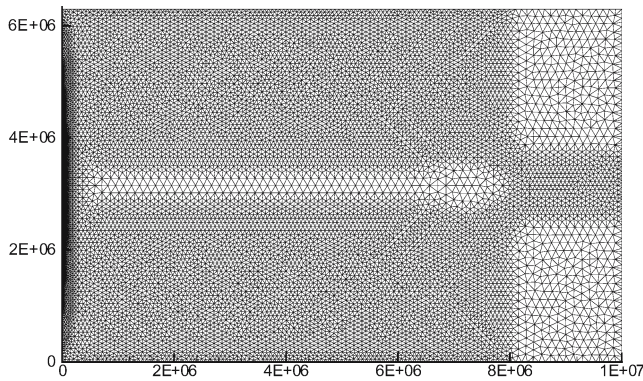


Fig. 11 Stretched unstructured triangular grid used in the Stommel Gyre case

CPU times of VELA should increase. Our experience with estuarine applications suggest that the CPU time should increase by a factor of 2.

The use of the minmod slope limiter and modified minmod (TVBM) limiters increases computation times over the unlimited RKDG schemes considerably. The relatively long computation times of MLG and MUST are also largely attributable to the slope limiters they employ. TG takes roughly double the computation time of GFEM and SUPG because it uses half the time step of these schemes. Because FE-FCT uses TG as the high-order scheme, the FE-FCT time step is half that of

Fluct. Redis., thus, accounting for much of the relative computational efficiency of Fluct. Redis. over FE-FCT.

5 Discussion and summary

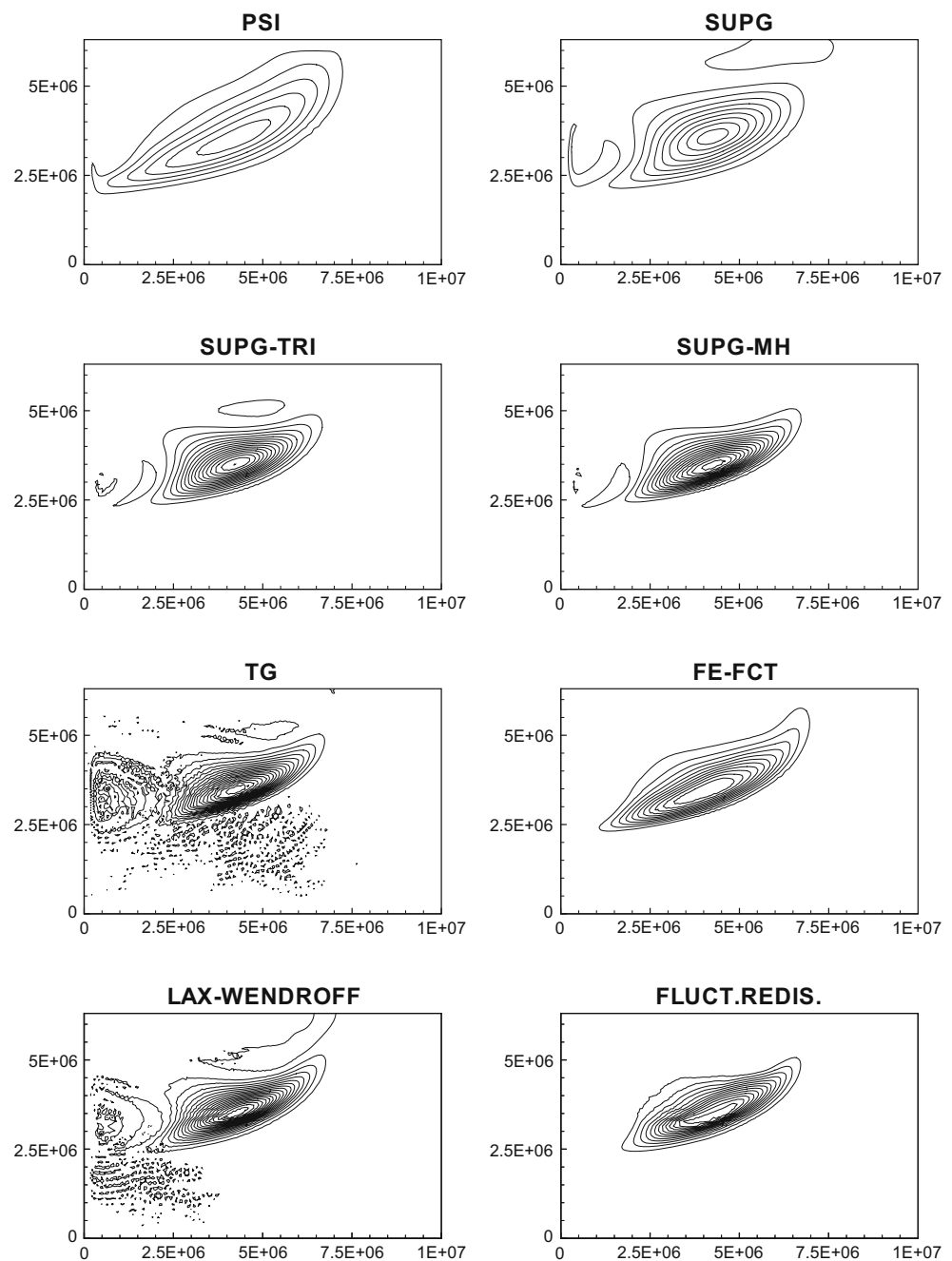
In this study, the behavior of a variety of advection schemes for unstructured grids is examined on a number of test cases. From the results, it is clear that the new ELM methods, which minimize mass errors and oscillations, such as VELA and its monotonic variants (VELA-FCT and VELA-NLF), possess the highest accuracy of the schemes examined. ELM schemes are ideal for passive tracer studies in which large time steps can be used. However, the complexity of the space-time control volume formulation of these new ELMs might prove an obstacle for problems dealing with space- and time-varying boundary conditions. Although these types of boundary conditions have been implemented in similar models (ELLAMs, Binning and Celia (1996)), the complexity of dealing with unstructured grids and complex boundaries in coastal problems in a mass-preserving way may lead to significant increases in CPU time.

The RKDG3 scheme is nearly as accurate as the VELA family. Whereas the scheme is computationally

Table 7 Stommel gyre on the stretched mesh test case results

Advection scheme	MIN	MAX	l_2	V	TV
GFEM	–	–	–	–	–
NQ-RK2	–	–	–	–	–
NQ-EF	–	–	–	–	–
SUPG	–0.031	–0.521	0.467	–0.538	–0.309
SUPG-Tri	–0.020	–0.200	0.181	–0.189	–0.093
SUPG-MH	–0.027	–0.172	0.159	–0.163	–0.026
TG	–0.066	–0.054	0.106	–0.028	0.931
PSI	0.000	–0.667	0.630	–0.662	–0.304
FE-FCT	0.000	–0.412	0.377	–0.349	–0.081
Lax-Wendroff	–0.080	–0.066	0.149	–0.056	0.546
Fluct. Redis.	0.000	–0.327	0.280	–0.320	–0.087
VELA $NT = 30$	–0.002	0.000	0.015	0.005	0.028
VELA $NT = 4$	–0.003	0.004	0.017	0.007	0.025
VELA-FCT $NT = 30$	0.000	–0.014	0.016	0.003	0.018
VELA-FCT $NT = 4$	0.000	0.003	0.017	0.007	0.015
VELA-NLF $NT = 30$	0.000	–0.015	0.045	–0.010	0.031
VELA-NLF $NT = 4$	0.000	0.003	0.023	0.007	0.024
MLG	0.000	–0.562	0.575	–0.582	–0.115
MUST	0.000	–0.014	0.434	0.544	0.178
RKDG2	–0.029	–0.101	0.131	–0.084	0.006
RKDG2-minmod	0.000	–0.460	0.446	–0.474	–0.119
RKDG2-TVBM	–0.003	–0.416	0.412	–0.430	–0.088
RKDG3	–0.004	0.006	0.018	0.019	0.012
RKDG3-minmod	0.000	–0.452	0.434	–0.447	–0.103
RKDG3-TVBM	–0.003	–0.411	0.407	–0.420	–0.081

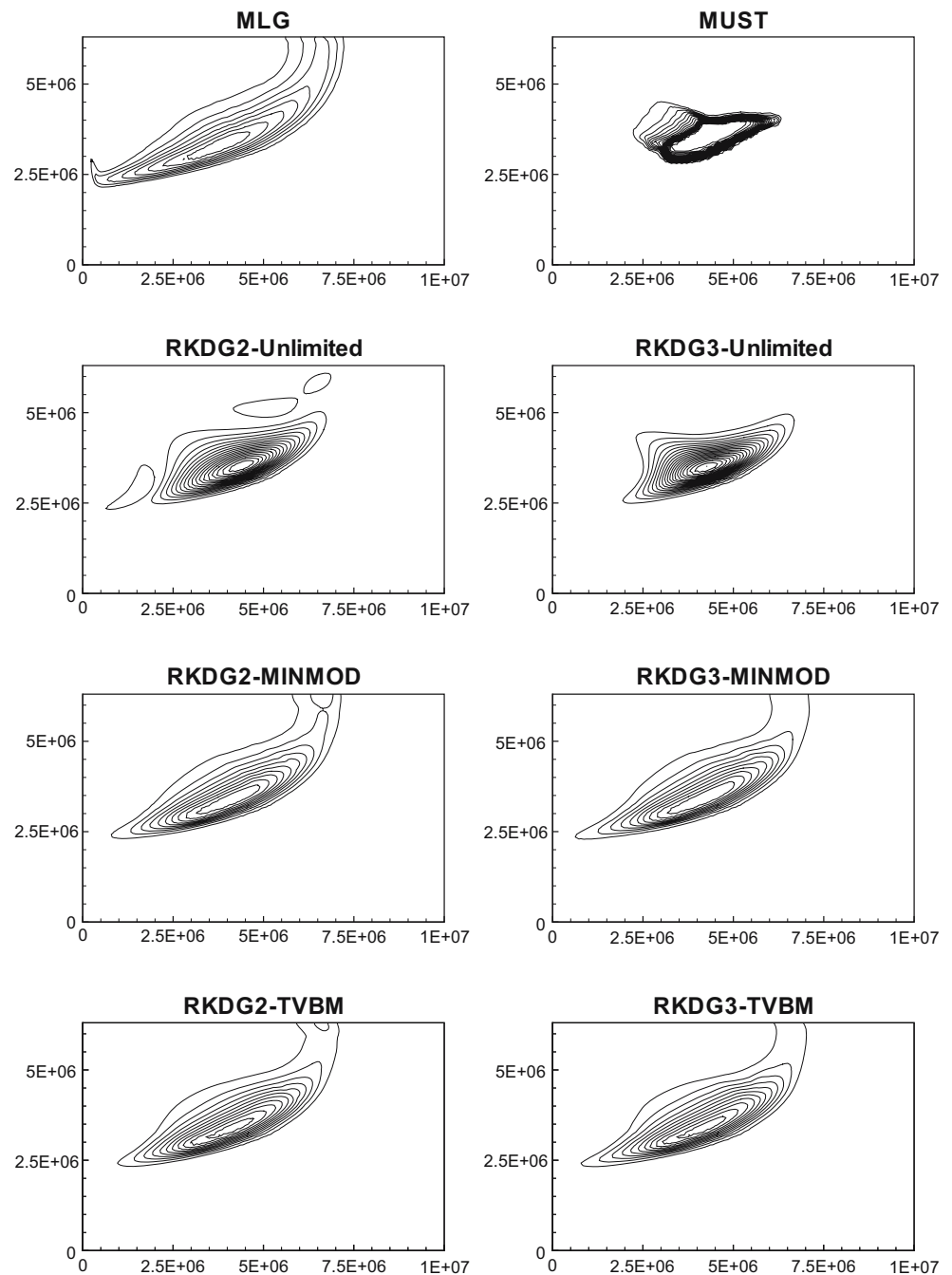
Fig. 12 Concentrations at $t = 1.5 \times 10^8$ s for advection schemes in the Stommel gyre test case with a variable mesh



expensive relative to nearly all the other schemes, Cockburn and Shu (1998) note that the third-order convergence rate of RKDG3 means that the scheme can achieve better accuracy than the second-order schemes at much coarser resolution and, thus, lower computational cost. The RKDG3 scheme is not monotonic, but at moderate to high resolution, the negative undershoot is nearly negligible. If strict monotonicity is required, a minmod slope limiter can be applied but at a cost of reducing the order of the scheme to less than second

order and a tripling of the computation time. This is in contrast to the VELA-FCT and VELA-NLF schemes, which produce monotonic results with no loss in accuracy and negligible increase in computation time. The TVBM limiter may provide a compromise between the high-accuracy non-monotonic RKDG3 and the low-order monotonic RKDG3-minmod, but in practice, it proved difficult to find generally appropriate values for the weighting parameter. The success of the nonlinear monotonicity-preserving filter in VELA-NLF suggests

Fig. 13 Concentrations at $t = 1.5 \times 10^8$ s for advection schemes in the Stommel gyre test case with a variable mesh



that a similar filtering operation applied to RKDG3 might achieve monotonicity in that scheme at reasonable computational cost.

Overall, TG and RKDG2 perform better than the other second-order schemes. These two schemes produce less undershoot and fewer dispersive ripples while maintaining higher accuracy than the other second-order schemes.

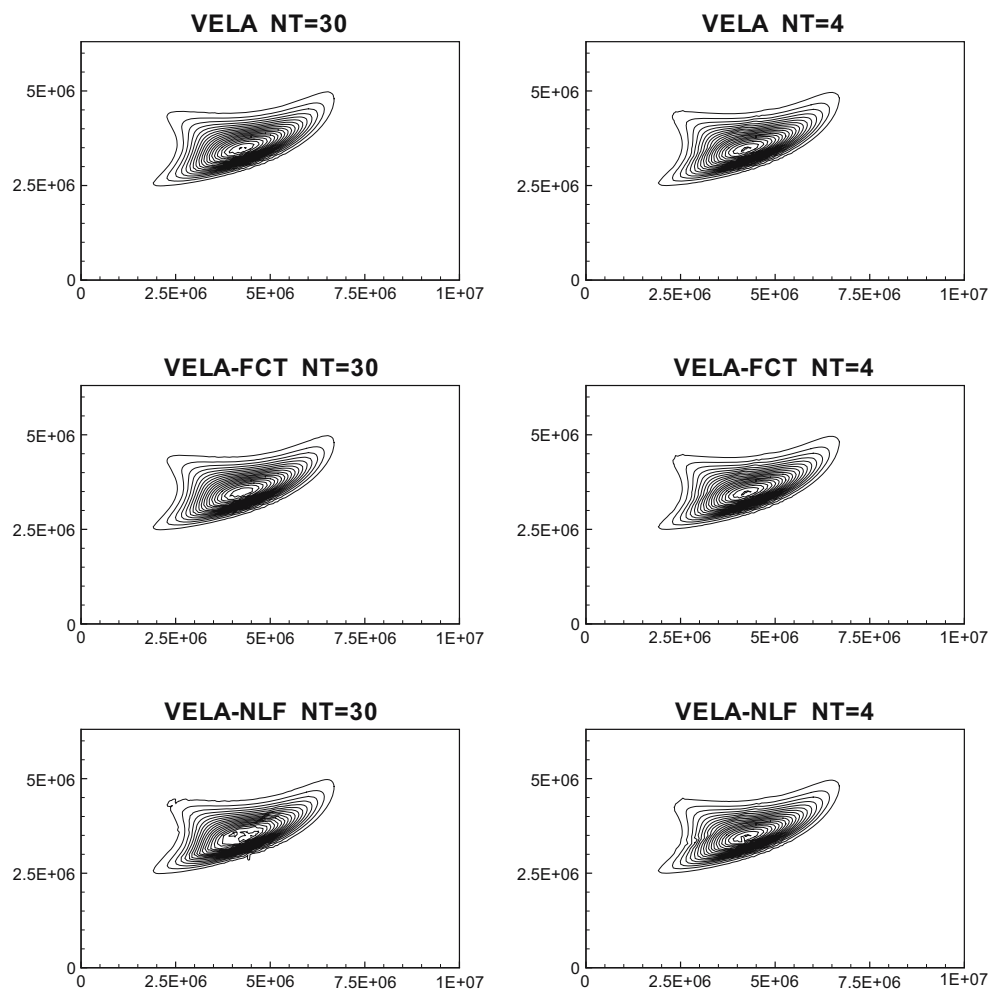
Of the monotonic (nominally) second-order schemes, Fluct. Redis. and FE-FCT provide similar results. On the most realistic test case, that of the Stommel Gyre

on a variable mesh, however, Fluct. Redis. emerges as superior to FE-FCT. Furthermore, the Fluct. Redis. scheme is over twice as fast as FE-FCT.

The MLG and MUST schemes, while monotonic, proved to be first-order accurate and computationally expensive. MLG severely attenuated peak concentrations, while MUST greatly distorted the shape of the concentration distribution by producing excessively steep gradients.

While the along-stream diffusion implicit in SUPG attenuated peak concentrations below that of TG and

Fig. 14 Concentrations at $t = 1.5 \times 10^8$ s for advection schemes in the Stommel gyre test case with a variable mesh



RKDG2, it was not sufficient to avoid negative undershoot in the concentration fields. SUPG–MH produced greater peak attenuation than SUPG in the rotating cone test, but created only negligible negative undershoot. SUPH–Tri was more dissipative than SUPG–

MH in the cone test, but produced the same level of negative undershoot. On the variable mesh Stommel Gyre problem, SUPG–MH and SUPG–Tri are superior to SUPG in every respect and are competitive with the second-order schemes. GFEM and TG provided

Table 8 Times relative to PSI in ascending order for rotating cone test case on 65×65 grid

Advection scheme	Relative time	Advection scheme	Relative time
MPDATA2 non-oscillatory	0.46	TG	6.73
Lax–Wendroff	0.52	RKDG2	8.61
MPDATA3 non-oscillatory	0.97	FE-FCT	10.66
PSI	1.00	RKDG–TVBM	12.83
NQ-RK2	1.44	VELA (NT = 50)	13.18
GFEM	2.73	VELA–NLF (NT = 50)	13.23
NQ-EF	2.85	VELA–FCT (NT = 50)	13.27
SUPG–MH	3.33	MLG	13.61
SUPG	3.44	MUST	14.10
SUPG–Tri	3.70	RKDG2–minmod	16.19
Fluct. Redis.	4.05	RKDG3	122.52
VELA–FCT (NT = 5)	4.37	RKDG3–TVBM	314.95
VELA (NT = 5)	4.41	RKDG3–minmod	318.66
VELA–NLF (NT = 5)	4.41		

acceptable accuracy for smooth gradient problems but introduced large errors for tests with sharp gradients.

To our knowledge, only the Hanert et al. (2004) study has compared unstructured triangular advection schemes on the Stommel gyre problem. Their results for continuous finite element, discontinuous finite element and finite volume schemes are consistent with the results presented in this paper for SUPG, RKDG2, and Lax-Wendroff, respectively.

The benefit of using unstructured grid approaches is the possibility employing of local mesh refinement. It is for that reason that the variable mesh Stommel Gyre test case is so important. It permits us to examine the behavior of the candidate schemes on a variable mesh where the advecting velocity field is representative of that encountered in typical basin-scale ocean model applications. The results from that test, in combination with the rest of the analyses of this study, lead us to recommend that for tracer studies, the VELA family of schemes should be considered. If non-negative fields are essential, then the VELA-FCT and VELA-NLF approaches can be adopted. Of the two, VELA-FCT provides better results. If slight negative undershoot is acceptable, then RKDG3 is also an excellent candidate scheme for tracer advection. TG and RKDG2 show the best overall performance of the second-order schemes. If non-negativity is an important property, then Fluct. Redis. should be considered. It is an accurate, computationally efficient scheme that is readily retro-fitted to existing finite element model codes.

Acknowledgements This work was supported in part by the Research Council of Norway, contract number 133109/431, and by Thayer School of Engineering, Dartmouth College, through funding provided by the US National Oceanic and Atmospheric Administration. The second author was sponsored by the Fundação para a Ciência e a Tecnologia, project Protecção e Valorização da Zona Costeira Portuguesa and by the Laboratório Nacional de Engenharia Civil, project Modelação Matemática de Processos Estuarinos e Costeiros. We wish to thank Professor D. R. Lynch for his support and encouragement through the course of this project and to Professor B. Cockburn for advice on the implementation of the RKDG schemes.

Appendix 1: Description of advection schemes

This section is a description of the advection schemes listed in Section 2.

1.1 Galerkin finite element

Included under Galerkin finite element schemes is the 'classic' Galerkin finite element scheme (GFEM) (see Finlayson (1992) or Morton (1996) for a deriva-

tion). GFEM employs the full, consistent mass matrix and centered, implicit (Crank-Nicolson) second-order time discretization. Maintaining the full, or consistent, mass matrix can be computationally expensive, as a large number of equations must be solved simultaneously through either direct or iterative means. Thus, there is a strong temptation to perform nodal quadrature, or mass lumping, to reduce the mass matrix to a diagonal through a summation of the contributions from surrounding nodes at each node. The lumped mass treatment, when combined with a second order Runge-Kutta time discretization, provides second-order accuracy in time and space while remaining computationally inexpensive enough for use in three-dimensional models. This scheme, denoted the nodal quadrature Galerkin, second-order Runge-Kutta (NQ-RK2), is included to examine the impact of mass lumping on the quality of advection results. Computation time can potentially be halved by employing the single time level first-order Euler forward scheme, denoted nodal quadrature Galerkin Euler forward (NQ-EF), to the lumped system. This scheme is examined, as it is currently in use in the existing three-dimensional finite element ocean model Quoddy (Lynch and Werner 1991), and we wished to determine the degradation in accuracy (if any) caused by employing first-order vs second-order time discretization. An approach that requires only a single time level while maintaining second-order accuracy in time and space is the Taylor-Galerkin method, denoted TG (Donéa 1984), which bears a close resemblance to the Lax-Wendroff schemes of the finite difference world. In this study, the TG scheme was applied with a consistent mass matrix.

1.2 Stabilized Galerkin methods

To minimize unwanted oscillatory behavior in Galerkin solutions, attempts have been made to stabilize the results by means of altering the variational formulation. Such approaches, known as stabilized methods, attempt to penalize spurious oscillations through means such as modification of the weighting function (Brooks and Hughes 1982), imposing a least squares penalty function (Hughes et al. 1989), or utilization of a residual-free bubble function in which a higher-order polynomial weighting function is used, which vanishes at the element boundaries (Brezzi et al. 1992; Hughes 1995). In this study, only variants of the streamline-upwind Petrov-Galerkin (SUPG) scheme will be considered, as for pure advection, the Galerkin least-squares formulation reduces to that of the SUPG (Ilinca et al. 2000) as do residual-free bubble stabilization schemes (Franca et al. 1998). The streamline-

upwind Petrov–Galerkin (SUPG) scheme (Brooks and Hughes 1982) applies an upwind weighting to obtain stable solutions in advection-dominated flows. In one dimension, the determination of an upstream direction is unambiguous and optimal in that it leads to nodally exact solutions. In two dimensions, however, the determination is more ambiguous, particularly on a triangular mesh. Mizukami (1985) developed a scheme for determining the upstream direction that is based on element properties that are defined unambiguously. The values of upstream direction and resulting element diffusivity vary with element nodes. This scheme of Mizukami (1985) is denoted SUPG–Tri. Mizukami and Hughes (1985) noted that the streamline is not always the appropriate upstream direction. They develop a Petrov–Galerkin scheme, denoted in this study as SUPG–MH, based on a discrete maximum principle that provides improved discontinuity, capturing while minimizing spurious oscillations. A consistent mass matrix and Crank–Nicolson time discretization was employed for all the SUPG schemes.

1.3 Fluctuation distribution

Within recent years, fluctuation distribution schemes have received increasing interest in computational fluid mechanics. The approach, described by Struijs (1993), entails the distribution of a cell update among the nodes connected to the cell. If the distribution of the update at a time step, or fluctuation, between the nodes is such as to produce an upwind weighting, the positive streamwise invariant (PSI) scheme is produced (Deconinck et al. 1994). While the PSI scheme is second order in the cross-stream direction and monotonic, it is only first order in the along-stream direction for transient problems. By centering the distribution of the fluctuation between nodes, one can generate the single time step, second-order Lax–Wendroff fluctuation distribution scheme (Deconinck et al. 1994). While the Lax–Wendroff scheme is second order, it is not monotonic and is subject to oscillatory behavior. To obtain monotonic solutions while maintaining second-order accuracy in smooth regions, Hubbard and Roe (2000) developed a fluctuation redistribution (Fluct. Redis.) scheme. This approach combines the first-order, but monotonic PSI scheme, with the second-order, but oscillatory Lax–Wendroff discretization. The approach can be viewed as a generalized flux-corrected transport algorithm, where the maximum non-oscillatory component of the fluctuation is obtained through a geometric projection.

There now exists a version of the PSI scheme that is both second-order accurate in space and time, as well

as positive (Abgrall and Mezine 2003), which appears promising. Unfortunately, we learned of this scheme too late for it to be included in this study.

1.4 Flux-corrected transport

As is well known, second-order methods such as the standard Galerkin and Taylor–Galerkin approaches will generate oscillatory behavior in the absence of diffusion in the presence of sharp concentration gradients. To maintain positive, monotonic solutions in the presence of strong advection, flux-corrected transport (FCT) algorithms can be employed. Löhner et al. (1987) developed a finite element FCT method that combines a higher-order scheme (a second-order Taylor–Galerkin with a consistent mass matrix) and a low-order solution (a lumped-mass Taylor–Galerkin with added diffusion). In this study, the finite element flux-corrected transport algorithm (FE-FCT) employs the consistent mass matrix Taylor–Galerkin scheme as the high-order approximation and the low-order scheme employed is the PSI approach, described in the previous section. The development of the scheme follows that for finite differences by Zalesak (1979), where ‘fluxes’ are replaced by ‘element contributions to a node.’

1.5 Cell-centered finite volume

MUSCL (monotone upstream-centered schemes for conservation laws; van Leer 1979) type schemes for cell-centered, triangular, finite volume approaches (Hubbard 1999) were investigated in this study. The governing equation is the flux conservative form of the advection equation as given in Eq. 19.

$$\frac{\partial c}{\partial t} + \nabla \cdot \mathbf{f}(c) = 0 \quad (19)$$

where $\mathbf{f}(c)$ is the flux vector, and in this study, is defined as $\mathbf{f}(c) = \mathbf{u}c$. Fluxes are summed across the cell faces, ensuring local mass conservation. To achieve higher-order accuracy, a reconstruction is performed across the cell and surrounding cells. In this case, linear reconstruction is employed to obtain second-order accuracy. The reconstructed solution, however, is not monotonic so that some sort of limiting operation, such as slope limiting, is applied when monotonicity is required. The maximum limited gradient (MLG) scheme of Batten et al. (1996) determines a reconstruction based on the concentration gradients in a cell and its three neighbors. The MLG gradient is then taken to be the largest, after slope limiting, of the four concentration gradients. In one dimension, the MLG reduces to the Superbee

limiter (Sweby 1984). A second-order upwind scheme on cell-centered triangular finite volumes has been developed by Tamamidis (1995). The method, designated MUST for monotonic upwind scheme for triangles, is fully upwind and formally second order. The solution is partitioned into first-order upwind and higher (second) order contributions. The second-order term is based on a reconstruction procedure in which values at the triangle vertices are computed through an inverse distance weighted summation of the surrounding barycenter values. The reconstructed vertex values are used to compute gradients across the triangles, but only the gradient upwind of a given cell face is used. The scheme is thus fully upwind. To ensure monotonicity, the higher-order contribution is limited so that the value at a cell face always lies between the values at the barycenters of the two connecting triangular cells. Time integration in both MLG and MUST is accomplished through a second-order Runge–Kutta scheme.

1.6 Discontinuous Galerkin

The discontinuous Galerkin scheme for multidimensions (Cockburn et al. 1990) is based on the flux-conservative form of the advection Eq. 19. As in the cell-centered finite volume schemes, fluxes are summed across element faces to produce cell mass conservation. However, higher-order reconstruction is based upon a Galerkin representation within each cell. If linear basis functions are used, then a lumped-mass time derivative can be employed, and second-order Runge–Kutta time integration can be applied to produce the second-order Runge–Kutta discontinuous Galerkin method (Cockburn and Shu 1998), which is denoted in this study as RKDG2. A third-order scheme, denoted RKDG3, is obtained by employing quadratic basis functions and third-order Runge–Kutta time integration. Mass lumping can not be used with the quadratic basis functions, however, and a 6×6 mass matrix must be decomposed for each element. The RKDG methods outlined above will not be free of oscillations. Slope limiting is applied to deal with this problem. In this study, the minmod and total variance bounded in the means (TVBM) slope limiters described by Cockburn et al. (1990) are employed.

1.7 Eulerian–Lagrangian methods

Eulerian–Lagrangian methods (ELMs) have become increasingly popular in a variety of fields (Binning and Celia 1996; Rasch and Williamson 1990; Sorek 1988; Staniforth and Côté 1991), combining the accuracy of the Lagrangian approach with the convenience of a

fixed computational grid. ELMs, however, can have serious mass conservation errors (Baptista 1987; Russell 1989), which are related to the accuracy of the tracking of the characteristic lines and of the evaluation of the integrals at the feet of the characteristic lines, to the mass conservation of the forcing flow field and to the implementation of the boundary conditions. To overcome these problems, several techniques have been proposed (Celia et al. 1990; Cheng et al. 1999; Oliveira and Baptista 1998; Oliveira et al. 2000). Among these, the Eulerian Lagrangian adjoint methods (ELLAMS) (Binning and Celia 1996; Celia et al. 1990; Russell 1989) have emerged as a distinct type of ELM methods based on space-time varying weighting functions, based on the adjoint equation. These methods allow for a mass conservative implementation of any type of boundary conditions. A control-volume finite element Eulerian–Lagrangian scheme, designated VELA (Oliveira 1997), is used in this study. This scheme presents some similarities with the ELLAM of Healy and Russell (1993), combining the finite volume approach for the integration of the transport equation, a high accuracy tracking and integration at the feet of the characteristic lines for best mass conservation. Although it also uses space-time weighting functions, this scheme does not resort to the adjoint of the equation, thus, separating the definition of the weighting function from the specific equation being solved. Concentrations and total depths are defined by linear shape functions in each element. The area integrals at the feet of the characteristic lines are evaluated by subdivision quadrature (Healy and Russell 1993; Oliveira 1997). Because the original VELA scheme produced significant oscillations in the presence of complex flow fields and large gradients (Oliveira 1997), two additional VELA-based schemes that eliminate oscillations are also presented in this study. The VELA–FCT (Oliveira and Fortunato 2002) is based on flux-corrected transport concepts adapted for finite elements (Löhner et al. 1987). Because the strict application of FCT concepts in ELMs will lead to mass errors (Priestley 1993), this scheme resorts to local mass correction techniques to eliminate mass errors without introducing excessive numerical damping. The third scheme (VELA–NLF), (Oliveira and Fortunato 2000, 2002) is based on the use of non-linear filters to eliminate oscillations, following the concepts proposed by Mahlman and Sinclair (1973). The VELA–NLF is an adaptation of the non-linear filter of Mahlman and Sinclair (1973) for unstructured grids and is based on mass conservation concepts to eliminate the oscillations. Once an oscillation is found, the concentrations at this node and at the adjacent node that leads to the maximum concentration

difference are set to be equal by preventing any mass changes in the set of elements that contain any of the two nodes.

1.8 MPDATA

The multidimensional positive definite advection transport algorithm (MPDATA) (Smolarkiewicz 1984; Smolarkiewicz and Clark 1986; Smolarkiewicz and Grabowski 1990; Smolarkiewicz and Margolin 1998) is a second-order accurate, positive-definite, and conservative finite-difference advection scheme commonly used in geophysical fluid applications. MPDATA is an iterative scheme in which the first pass is a donor cell, or upstream differenced, approximation that is positive definite but only first-order accurate. The second pass estimates and approximately compensates for the second-order truncation error of the first pass. Successive additional passes estimate the error of the previous pass and approximately correct for it, progressively improving the accuracy. In the first donor cell pass, the velocity is the actual physical velocity. In successive passes, the velocity is a pseudo- or anti-diffusive velocity, which is calculated from the field being advected and possesses no physical significance. MPDATA is positive definite (sign preserving), but not monotonic. To eliminate spurious oscillations, a non-oscillatory option was developed (Smolarkiewicz and Grabowski 1990) that uses flux limiting to impose monotonicity. In this study, only the non-oscillatory version of MPDATA is used, with two and three iterative passes, denoted MPDATA-2 and MPDATA-3, respectively.

References

- Abgrall R, Mezine M (2003) Construction of second order accurate monotone and stable residual distribution schemes for unsteady flow problems. *J Comput Phys* 188:16–55
- Baptista AM (1987) Solution of advection-dominated transport by Eulerian–Lagrangian methods using the backwards method of characteristics. PhD thesis, Massachusetts Institute of Technology, Cambridge, MA, USA
- Batten P, Lambert C, Causon DM (1996) Positively conservative high-resolution convection schemes for unstructured elements. *Int J Numer Methods Fluids* 39:1821–1838
- Binning P, Celia MA (1996) An Eulerian–Lagrangian localized adjoint method for solution of the contaminant transport equations in two-dimensional multiphase flow systems. *Water Resour Res* 32:103–114
- Bleck R, Rooth C, Hu D, Smith LT (1992) Salinity-driven thermocline transients in a wind- and thermohaline-forced isopycnal model of the north atlantic. *J Phys Oceanogr* 22: 1486–1505
- Brezzi F, Bristeau O, Franca LP, Mallet M, Roge G (1992) A relationship between stabilized finite element methods and the galerkin method with bubble functions. *Comput Methods Appl Mech Eng* 96:117–129
- Brooks AN, Hughes TJR (1982) Stream-line upwind/Petrov–Galerkin formulation for convection dominated flows with particular emphasis on the incompressible Navier–Stokes equations. *Comput Methods Appl Mech Eng* 32:199–259
- Budgell WP, Skogen MD (2000) Advection schemes for coastal ocean models, Fisker og Havet 3-2000. Institute of Marine Research, Bergen, Norway
- Celia MA, Russell TF, Herrera I, Ewing RE (1990) An Eulerian–Lagrangian localized adjoint method for the advection–diffusion equation. *Adv Water Resour* 13:187–206
- Chen C, Beardsley RC (2002) Cross-frontal water exchange on georges bank: some results from an US GLOBEC/Georges Bank Program model study. *J Oceanogr* 58:403–420
- Cheng JR, Cheng HP, Yeh GT (1999) A Lagrangian–Eulerian method with adaptively local zooming and peak/valley capturing approach to solve two-dimensional advection–diffusion transport equations. *Int J Numer Methods Fluids* 39:987–1016
- Cockburn B, Shu CW (1998) The Runge–Kutta discontinuous Galerkin finite element method for conservation laws V: multidimensional systems. *J Comput Phys* 141:199–224
- Cockburn BS, Hou S, Shu CW (1990) TVB Runge–Kutta local projection discontinuous Galerkin finite element method for conservation laws IV: the multidimensional case. *Math Comput* 54:545–581
- Curchitser EN, Haidvogel DB, Iskandarani M (2001) Transient adjustment of circulation in a midlatitude abyssal ocean basin with realistic geometry and bathymetry. *J Phys Oceanogr* 31:725–745
- Deconinck H, Strujis R, Bourgois G, Roe PL (1994) High resolution shock capturing cell vertex advection schemes for unstructured grids. In: *Computational fluid dynamics*
- Donéa, J (1984) A Taylor–Galerkin method for convective transport systems. *Int J Numer Math Eng* 20:101–119
- Finlayson BA (1992) *Numerical methods for problems with moving fronts*. Ravenna Park Publishing, Seattle
- Franca LP, Farhat C, Lesoinne M, Russo A (1998) Unusual stabilized finite element methods and residual free bubbles. *Int J Numer Methods Fluids* 27:942–958
- Godlewski E, Raviart PA (1996) *Numerical approximation of hyperbolic systems of conservation laws*. Springer-Verlag, New York
- Greenberg DA, Werner FE, Lynch DR (1998) A diagnostic finite-element ocean circulation model in spherical-polar coordinates. *J Atmos Ocean Technol* 15:159–168
- Hanert E, Le Roux DY, Legat V, Deleersnijder E (2004) Advection schemes for unstructured grid ocean modelling. *Ocean Model* 7:39–58
- Hannah CG, Shore JA, Loder JW (2001) Seasonal circulation on the western and central scotian shelf. *J Phys Oceanogr* 31:591–615
- Suginohara N, Hasumi H (1999) Sensitivity of a global ocean general circulation model to tracer advection schemes. *J Phys Oceanogr* 29:2730–2740
- Healy RW, Russell TF (1993) A finite-volume Eulerian–Lagrangian localized adjoint method for the solution of the advection–dispersion equation. *Water Resour Res* 29: 2399–2413
- Hecht MW, Holland, WR, Rasch PJ (1995) Upwind-weighted schemes for ocean tracer transport: an evaluation in a passive tracer context. *J Geophys Res* 100:3301–3321
- Hecht MW, Wingate BA, Kassis P (2000) A better, more discriminating test problem for ocean tracer transport. *Ocean Model* 2:1–15

- Higdon RL (2002) A two-level time-stepping method for layered ocean circulation models. *J Comput Phys* 177:59–94
- Hirsch C (1990) Numerical computation of internal and external flows, vol. 2. Computational methods for inviscid and viscous flows. Wiley, New York
- Hubbard ME (1999) Multidimensional slope limiters for MUSCL-type finite volume schemes on unstructured grids. *J Comput Phys* 155:54–74
- Hubbard ME, Roe PL (2000) Compact high-resolution algorithms for time-dependent advection on unstructured grids. *Int J Numer Methods Fluids* 33:711–736
- Hughes TJR (1995) Multiscale phenomena: Green's functions, the Dirichlet-to-Neumann formulation, subgrid scale models, bubbles and the origin of stabilized methods. *Comput Methods Appl Mech Eng* 127:387–401
- Hughes TJR, Franca LP, Hulbert GM (1989) A new finite element formulation for computational fluid mechanics: VIII. The Galerkin-least-squares method for advective-diffusive equations. *Comput Methods Appl Mech Eng* 73:173–189
- Ilinca F, Hétu J-F, Pelletier D (2000) On stabilized finite element formulations for incompressible advective-diffusive transport and fluid flow problems. *Comput Methods Appl Mech Eng* 188:235–255
- Iskandarani M, Haidvogel DB, Boyd JP (1995) A staggered spectral element model with application to the oceanic shallow-water equations. *Int J Numer Methods Fluids* 20:393–414
- Kröner D (1997) Numerical schemes for conservation laws. Wiley-Teubner, Chichester
- Le Provost C, Genco ML, Lyard F, Vincent P, Canceil P (1994) Spectroscopy of the world ocean tides from a finite-element hydrodynamic model. *J Geophys Res* 99:24777–24797
- Le Roux DY, Staniforth A (2000) A semi-implicit semi-Lagrangian finite-element shallow-water ocean model. *Mon Weather Rev* 128:1384–1401
- LeVeque RJ (1992) Numerical methods for conservation laws. Birkhäuser Verlag, Basel
- LeVeque RJ (2002) Finite volume methods for hyperbolic problems. Cambridge University Press, Cambridge
- Levin JG, Iskandarani M, Haidvogel DB (2000) A nonconforming spectral element ocean model. *Int J Numer Methods Fluids* 34:495–525
- Löhner R, Morgan K, Peraire J, Vahdati M (1987) Finite element flux-corrected transport (FEM-FCT) for the Euler and Navier-Stokes equations. *Int J Numer Methods Fluids* 7:1093–1109
- Lynch DR, Hannah CG (2001) Inverse model for limited-area hindcasts on the continental shelf. *J Atmos Ocean Technol* 18:962–981
- Lynch DR, Ip JTC, Naimie CE (1996) Comprehensive coastal circulation model with application to the Gulf of Maine. *Cont Shelf Res* 16:875–906
- Lynch DR, Werner FE (1987) Three-dimensional hydrodynamics on finite elements. 1. Linearized harmonic model. *Int J Numer Methods Fluids* 7:871–909
- Lynch DR, Werner FE (1991) Three-dimensional hydrodynamics on finite elements. Part II: Non-linear time-stepping model. *Int J Numer Methods Fluids* 12:507–533
- Mahlman JD, Sinclair RW (1973) Tests of various numerical algorithms applied to a simple trace constituent air transport problem. In: Suffet I (ed) Fate of pollutants in the air and water environments, vol. 8. In: *Advances in Environmental Science and Technology*. Wiley-Interscience, New York
- Mizukami A (1985) An implementation of the streamline-upwind/Petrov-Galerkin method for linear triangular elements. *Comput Methods Appl Mech Eng* 49:357–364
- Mizukami A, Hughes TJR (1985) A Petrov-Galerkin finite element method for convection-dominated flows: An accurate upwinding technique for satisfying the maximum principle. *Comput Methods Appl Mech Eng* 50:181–193
- Morton KW (1996) Numerical solution of convection-diffusion problems. Chapman and Hall, London
- Oksuzoglu H, Hees AGM (1998) A barotropic ocean model and its parallel implementation on unstructured grids. *Lect Notes Comput Sci* 1401:125–132
- Oliveira A (1997) Eulerian-Lagrangian analysis of transport and residence times in estuaries and coasts. PhD thesis, Oregon Graduate Institute of Science and Technology, Portland, OR, USA
- Oliveira A, Baptista AM (1998) On the role of tracking on Eulerian-Lagrangian solutions of the transport equation. *Adv Water Resour* 21:539–546
- Oliveira A, Fortunato AB (2000) Non-linear filtering of numerical oscillations in two-dimensional unstructured grids. In: Brebbia Bentley, Sykes, Pinder (eds) *Computational methods in water resources XIII*, vol. 1, pp 381–388. Balkema, Cape Town
- Oliveira A, Fortunato AB (2002) Towards an oscillation-free, mass conservative, Eulerian-Lagrangian transport model. *J Comput Phys* 183:142–164
- Oliveira A, Fortunato AB, Baptista AM (2000) Mass balance in Eulerian-Lagrangian transport simulations in estuaries. *J Hydraul Eng* 126:605–614
- Priestley, A (1993) A quasi-conservative version of the semi-lagrangian advection scheme. *Mon Weather Rev* 121: 621–629
- Rasch PJ, Williamson DL (1990) On shape-preserving interpolation and semi-Lagrangian transport. *SIAM Sci J Stat Comput* 11:656–687
- Russell TF (1989) Eulerian-Lagrangian localized adjoint methods for advection-dominated problems. In: *Pitman Research Notes*, vol. 228, pp 206–228. Longman, New York
- Smolarkiewicz PK (1984) A fully multidimensional positive definite advection transport algorithm with small implicit diffusion. *J Comput Phys* 54:325–362
- Smolarkiewicz PK, Clark TL (1986) A fully multidimensional positive definite advection transport algorithm: further development and applications. *J Comput Phys* 67: 396–438
- Smolarkiewicz PK, Grabowski WW (1990) The fully multidimensional positive definite advection transport algorithm: Nonoscillatory option. *J Comput Phys* 86:355–375
- Smolarkiewicz PK, Margolin LG (1998) MPDATA: A finite-difference solver for geophysical flows. *J Comput Phys* 140:459–480
- Sorek S (1988) Eulerian-Lagrangian method for solving transport in aquifers. *Adv Water Resour* 11:67–73
- Staniforth A, Côté (1991). Semi-Lagrangian integration schemes for atmospheric models—a review. *Mon Weather Rev* 119:2206–2223

- Stommel H (1948) The westward intensification of wind-driven ocean currents. *Trans Am Geophys Union* 29:202–206
- Struijs R (1993) The fluctuation splitting method. In: Vreugdenhil CB, Koren B (eds) *Numerical methods for advection-diffusion problems*. Vieweg, Wiesbaden
- Sweby PK (1984) High resolution schemes using flux limiters for hyperbolic conservation laws. *SIAM J Numer Anal* 21: 995–1011
- Tamamidis P (1995) A new upwind scheme on triangular meshes using the finite volume method. *Comput Methods Appl Mech Eng* 124:15–31
- Toro EF (1999) *Riemann solvers and numerical methods for fluid mechanics*. Springer, Heidelberg
- Van Leer B (1979) Towards the ultimate conservative difference scheme V. A second order sequel to Godunov's method. *J Comput Phys* 32:101–136
- Vreugdenhil CB, Koren B (1993) *Numerical methods for advection-diffusion problems*. Vieweg, Braunschweig, Wiesbaden
- Zalesak ST (1979) Fully multidimensional flux-corrected transport algorithm for fluids. *J Comput Phys* 31: 335–362